contribute to the generation of nT reg cells in the thymus. However, how these cells contribute to and/or cooperate for the generation of nT reg cells is still elusive.

tDCs are predominantly accumulated in the medullary region of the thymus and sparsely detectable in the cortex (Barclay and Mayrhofer, 1981; Flotte et al., 1983; Kurobe et al., 2006). The accumulation of tDCs in the medulla is presumed to contribute to their efficient cooperation with mTECs in the establishment of negative selection and nT reg cell generation. Nonetheless, how tDCs are accumulated in the thymic medulla and how this medullary accumulation of tDCs contributes to negative selection and nT reg cell generation are unknown. The present study identifies the chemokine XCL1, also known as lymphotactin, as being essential for the medullary accumulation of tDCs. Cells that produce XCL1 in the thymus include mTECs, whereas XCR1, the receptor for XCL1, is expressed by tDCs. We also find that Aire is essential for the mTEC production of XCL1. In mice deficient for XCL1 or Aire, most tDCs fail to accumulate in the medulla and are arrested at the cortico-medullary junction (CMJ). The generation of nT reg cells is impaired in both *Xcl1*-deficient mice and *Aire*-deficient mice. Like *Aire*-deficient mice (Anderson et al., 2002, 2005), *nude* mice transferred with thymocytes from *Xcl1*-deficient mice exhibit inflammatory lesions in lacrimal glands. These results reveal that the XCL1-mediated medullary accumulation of tDCs critically contributes to the development of nT reg cells, and they suggest a role for Aire in facilitating the XCL1-mediated medullary accumulation of tDCs.

RESULTS

Screening for chemokines involved in the localization of tDCs

tDCs are predominantly accumulated in the medulla and sparsely detectable in the cortex (Barclay and Mayrhofer, 1981; Flotte et al., 1983; Kurobe et al., 2006). To identify chemokines that mediate the medullary accumulation of tDCs, we screened for the expression of chemokine receptors in isolated tDCs by RT-PCR analysis. Among the mouse chemokine receptors so far identified, *Ccr2*, *Ccr4*, *Ccr5*, *Ccr6*, *Ccr7*, *Ccr8*, *Cxcr1*, *Cxcr3*, *Cxcr4*, *Xcr1*, and *Cx3cr1* were detected in CD11c$^+$ cells isolated from the thymus (Fig. 1 A). We then examined chemokines that could bind to these transcript-detectable receptors for their ability to attract CD11c$^+$ thymic cells. We found that CCL19 (CCR7 ligand), CCL21 (CCR7 ligand), CXCL12 (CXCR4 ligand), or XCL1 (XCR1 ligand) attracted CD11c$^+$ thymic cells (Fig. 1 B). These results revealed the potential roles of CCR7, CXCR4, and XCR1 in the chemotactic regulation of tDCs. However, we detected no obvious defects in the medullary accumulation of CD11c$^+$ DCs in the thymus of mice deficient for CCR7, CCR7 ligands, or CXCR4 (Fig. 1 C; also see Fig. 3 D), even though the medullary region in CCR7- or CCR7 ligand–deficient mice was smaller than that in control mice (Fig. 1 C; Kurobe et al., 2006; Nitta et al., 2009). Thus, instead of CCR7 and CXCR4, the XCL1–XCR1 chemokine axis may play a major role in regulating the medullary accumulation of tDCs.

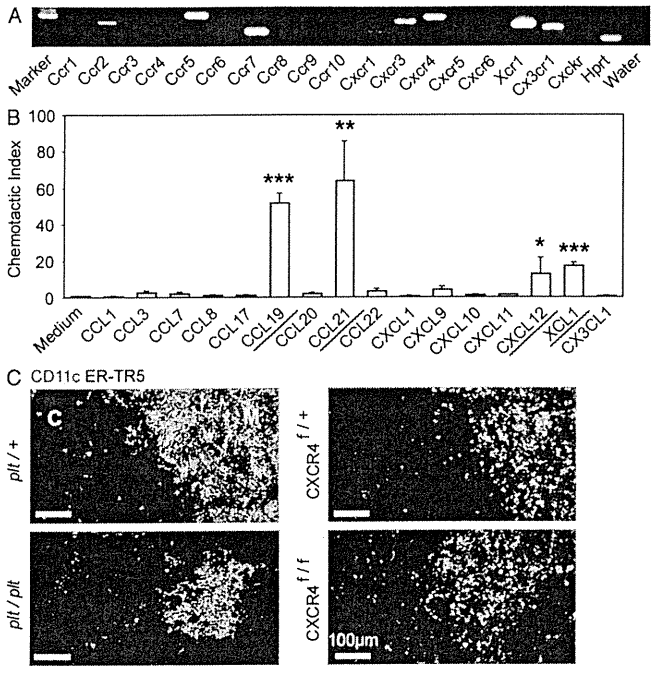

Figure 1. Screening for chemokines that regulate the localization of tDCs. (A) RT-PCR analysis of chemokine receptor expression in isolated tDCs. Shown are the results of ethidium bromide detection of electrophoretically separated PCR products. Hprt, hypoxanthine-guanine phosphoribosyltransferase. Shown are the representative data of three independent experiments. (B) Chemotactic indexes of tDCs to the ligands of expressed chemokine receptors CCL1 (CCR8 ligand), CCL3 (CCR5 ligand), CCL7 (CCR2 ligand), CCL8 (CCR5 ligand), CCL17 (CCR4 ligand), CCL19 (CCR7 ligand), CCL20 (CCR6 ligand), CCL21 (CCR7 ligand), CCL22 (CCR4 ligand), CXCL1 (CXCR1 ligand), CXCL9 (CXCR3 ligand), CXCL10 (CXCR3 ligand), CXCL11 (CXCR3 ligand), CXCL12 (CXCR4 ligand), XCL1 (XCR1 ligand), and CX3CL1 (CX3CR1 ligand) were determined. Bar graphs indicate means ± standard errors of the data from at least three independent measurements. Red underlines indicate the chemokines that attracted the tDCs (based on the statistical significance as shown in the graph). *, $P < 0.05$; **, $P < 0.01$; ***, $P < 0.001$. (C) Frozen thymus sections from CCR7 ligand–deficient (*plt/plt*) and CXCR4-deficient (Mx-Cre x CXCR4$^{f/f}$) mice, as well as the control mice, were stained with anti-CD11c antibody (green) and mTEC-specific antibody ER-TR5 (red). The majority, if not all, of *Cxcr4* was deleted in the thymus cells of Mx-Cre x CXCR4$^{f/f}$ mice. C, cortex; M, medulla. Shown are the representative results of three independent experiments.

Xcr1 expression by tDCs and *Xcl1* expression by mTECs

We next examined the expression of *Xcr1* and *Xcl1* in various cell populations in the thymus. We found that *Xcr1* transcripts in the thymus were detected exclusively in CD11c$^+$ tDCs and not in CD45$^+$ total thymocytes, CD11b$^+$CD11c$^-$ macrophages, or nonhematopoietic thymic stromal cells, including CD45$^-$I-A$^+$UEA1$^+$ mTECs and CD45$^-$I-A$^+$Ly51$^+$ cortical thymic epithelial cells (cTECs; Fig. 2 A). Among tDCs, *Xcr1* was most highly expressed in I-A^{high}CD11c^{high}CD11b$^-$ lymphoid DCs compared with I-A^{high}CD11c^{high}CD11b$^+$ myeloid DCs or I-A^{medium}CD11c^{medium}B220$^+$ plasmacytoid DCs (Fig. 2 B). Comparable amounts of *Xcr1* were detected in DCs from the thymus, spleen, subcutaneous lymph nodes,

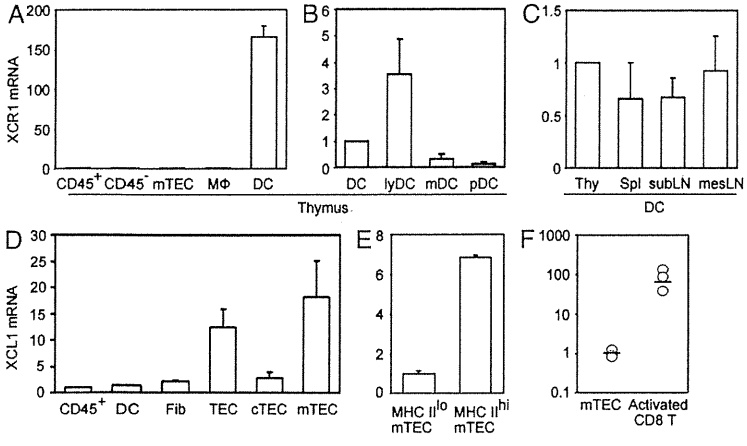

Figure 2. Expression of *Xcr1* and *Xcl1* in the thymus. (A–C) Quantitative RT-PCR analysis of *Xcr1* expression in sorted thymus cell populations, including CD45$^+$ thymocytes (CD45$^+$), CD45$^-$ thymic stromal cells (CD45$^-$), CD45$^-$I-A$^+$UEA1$^+$ mTECs, CD11b$^+$CD11c$^-$ macrophages (MΦ), and CD11c$^+$ tDCs (A); in sorted tDC subpopulations, including CD11c$^+$ total tDCs, I-A^{high}CD11c^{high}CD11b$^-$ lymphoid tDCs (lyDC), I-A^{high}CD11c^{high}CD11b$^+$ myeloid tDCs (mDC), and I-A^{medium}CD11c^{medium}B220$^+$ plasmacytoid tDCs (pDC) (B); and in CD11c$^+$ DCs from the thymus (Thy), the spleen (Spl), the subcutaneous lymph nodes (subLN), and the mesenteric lymph nodes (mesLN; C). The amounts of *Xcr1* were normalized to the amount of *Hprt*, and those in CD45$^+$ thymocytes (A) and total tDCs (B and C) were arbitrarily set to 1. (D and E) Quantitative RT-PCR analysis of *Xcl1* expression in thymus cell populations, including CD45$^+$ thymocytes (CD45$^+$), CD11c$^+$ DCs, CD45$^-$I-A$^-$MTS15$^+$ fibroblasts (Fib), CD45$^-$I-A$^+$ total TECs (TEC), CD45$^-$I-A$^+$Ly51$^+$ cTECs (cTEC), and CD45$^-$I-A$^+$UEA1$^+$ mTECs (mTEC); and in CD45$^-$I-A^{low}UEA1$^+$ (MHC II^{lo}) and CD45$^-$I-A^{high}UEA1$^+$ (MHC II^{hi}) mTEC subpopulations. The amounts of *Xcl1* were normalized to the amount of *Hprt*, and those in CD45$^+$ thymocytes (D) and CD45$^-$ I-A^{low}UEA1$^+$ mTECs (E) were arbitrarily set to 1. Bar graphs show means and standard errors of at least three independent measurements. (F) Quantitative RT-PCR analysis of *Xcl1* expression in CD45$^-$I-A$^+$UEA1$^+$ mTECs and anti-CD3–stimulated CD8$^+$ T cells. Means (bars) and individual measurements (circles) are shown (n = 3).

and mesenteric lymph nodes (Fig. 2 C). In contrast, *Xcl1* transcripts in the thymus were detected in CD45$^-$I-A$^+$UEA1$^+$ mTECs rather than CD45$^+$ thymocytes, CD11c$^+$ tDCs, CD45$^-$I-A$^-$MTS15$^+$ fibroblasts, or CD45$^-$I-A$^+$Ly51$^+$ cTECs (Fig. 2 D). Among the mTECs, *Xcl1* was prominently detected in CD45$^-$I-A^{high}UEA1$^+$ (MHC II^{hi}) mTECs rather than CD45$^-$I-A^{low}UEA1$^+$ (MHC II^{lo}) mTECs (Fig. 2 E). In addition to mTECs, *Xcl1* was also detected in a small subpopulation of CD45$^+$ thymocytes expressing NK1.1, including NK1.1$^+$CD3$^-$ NK cells and NK1.1$^+$CD3$^+$ NKT cells (Kelner et al., 1994; Hedrick et al., 1997; unpublished data). Previous studies showed that *Xcl1* is expressed in the secondary lymphoid organs by Th1-polarized CD4$^+$ T cells and activated CD8$^+$ T cells (Dorner et al., 2002, 2009). The expression of *Xcl1* in mTECs was lower than that in activated CD8$^+$ T cells (Fig. 2 F). However, in the thymus, XCL1 is prominently produced by a fraction of mTECs, whereas its receptor XCR1 is exclusively expressed by tDCs.

Role of *Xcl1* in medullary accumulation of tDCs

To examine whether XCL1 plays a role in the localization of tDCs, we generated *Xcl1*-deficient mice (Fig. S1). In the thymus of *Xcl1*-deficient mice, we found that the medullary region was not densely populated with CD11c$^+$ tDCs (Fig. 3 A). Measurement of tDC density in various regions of the thymus sections (Fig. S2 A) indicated that the number of tDCs per unit area in the middle medullary region (M region) was significantly ($P < 0.001$) decreased in *Xcl1*-deficient mice as compared with control mice, whereas the number of tDCs per unit area in the deep cortical region close to the CMJ (CMJ-C region) was significantly ($P < 0.01$) elevated in *Xcl1*-deficient mice as compared with control mice (Fig. 3, A and B). In contrast, the densities of tDCs in the subcapsular zone (SCZ) region, the middle cortical region (C region), and the peripheral medullary region close to the CMJ (CMJ-M region) were not significantly ($P > 0.05$) altered by the *Xcl1* deficiency (Fig. 3, A and B). Similarly to *Xcl1*-deficient mice of BALB/c background, *Xcl1*-deficient mice of C57BL/6 background exhibited altered distribution of tDCs, namely sparseness in the M region and density in the CMJ-C region (Fig. S2 B). Nonetheless, the absolute numbers of tDCs, including lymphoid DC, myeloid DC, and plasmacytoid DC subsets, were not affected in *Xcl1*-deficient mice (Fig. 3 C). These results indicate that XCL1 is essential for the accumulation of tDCs in the inner medullary region and that the deficiency of XCL1 causes the aberrant arrest of tDCs in the CMJ-C region.

The localization of tDCs was specifically altered in *Xcl1*-deficient mice but not in CCR7 ligand–deficient *plt/plt* mice or CXCR4-deficient mice (Fig. 1 C and Fig. 3 D). The defective accumulation of tDCs in the thymic medulla caused by the XCL1 deficiency was not further compromised by an additional lack of CCR7 ligands (Fig. 3 D). Thus, among the chemokines that exert chemotactic activity on tDCs (Fig. 1 B), XCL1 appears to be the major regulator of the tDC medullary accumulation.

Unlike tDCs, CD11b$^+$ macrophages in the thymus were not enriched in the medulla of WT mice but were most densely distributed in the CMJ-C region (Fig. 3, E and F). This distribution was not affected in *Xcl1*-deficient mice (Fig. 3, E and F). The distribution and number of CD4$^+$CD8$^+$, CD4$^+$CD8$^-$, or CD4$^-$CD8$^+$ thymocytes were normal in *Xcl1*-deficient mice (unpublished data). These results indicate that in the thymus, XCL1 influences the distribution of tDCs specifically.

Negative selection of self-reactive thymocytes in *Xcl1*-deficient mice

It was previously shown that tDCs contribute to the negative selection of self-reactive thymocytes (Jenkinson et al., 1992; Gallegos and Bevan, 2004). We therefore examined whether negative selection might be affected in the thymus

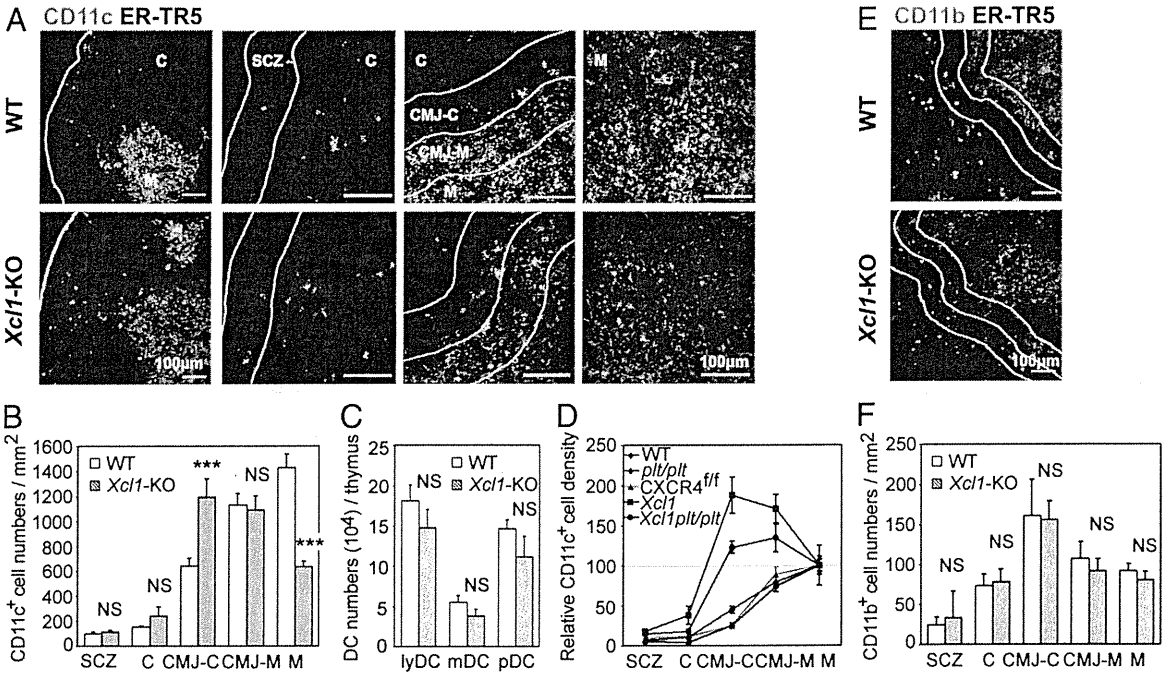

Figure 3. Distribution of DCs and macrophages in the thymus of *Xcl1*-deficient mice. (A) Two-color immunofluorescence analysis of thymus sections stained for CD11c (green) and the mTEC-specific ER-TR5 determinant (red). Representative images from three independent experiments are shown. White lines indicate borders among the indicated regions of the thymus section identified as in Fig. S2 A. C, cortex; M, medulla. Representative images from three independent experiments are shown. (B) Number of CD11c$^+$ cells per unit area (1 mm^2) of the indicated regions of the thymus sections was measured. Means and standard errors of cell numbers from three independent measurements are shown. (C) Means and standard errors (n = 6) of the absolute numbers of lymphoid DCs (lyDCs), myeloid DCs (mDCs), and plasmacytoid DCs (pDCs) in the thymus of indicated mice are shown. (D) Relative density of CD11c$^+$ cells in the indicated regions to the density in the medullary region of the thymus section (in percentile). Means and standard errors (n = 3) for WT, *plt/plt*, Mx-Cre × CXCR4$^{f/f}$, *Xcl1*-deficient, and *Xcl1*-deficient *plt/plt* mice are plotted. (E and F) The thymus sections were analyzed for CD11b (green) and the ER-TR5 determinant (red). Representative images from three independent experiments are shown in E, and means and standard errors of cell numbers from three independent analyses are shown in F. ***, $P < 0.001$. NS, not significant ($P > 0.05$).

of *Xcl1*-deficient mice. As tDCs have been implicated for their roles in negative selection by *mammary tumor virus* (*Mtv*)–encoded superantigens (Moore et al., 1994), we first analyzed the negative selection of Vβ3$^+$, Vβ5$^+$, and Vβ11$^+$ T cells in *Mtv*-expressing BALB/c mice. We found that the deletion of Vβ3$^+$ and Vβ5$^+$ TCR^{high} CD4$^+$CD8$^-$ thymocytes in the *Mtv*$^+$ BALB/c background, as compared with *Mtv*$^-$ C57BL/6 background, was slightly but significantly ($P < 0.05$) disturbed in *Xcl1*-deficient mice (Fig. 4 A). Meanwhile, Vβ3$^+$ and Vβ5$^+$ CD4$^-$CD8$^+$ thymocytes, as well as Vβ11$^+$ thymocytes in CD4$^+$CD8$^-$ and CD4$^-$CD8$^+$ subsets, were deleted comparably in BALB/c mice irrespective of the presence or absence of *Xcl1* (Fig. 4 A). Moreover, the deletion of Vβ3$^+$, Vβ5$^+$, and Vβ11$^+$ T cells detectable in the spleen was not defective in *Xcl1*-deficient BALB/c mice (Fig. S3). Thus, XCL1 plays a minor role in the negative selection of self-*Mtv*–reactive thymocytes.

We then examined whether negative selection of 2C-TCR–transgenic thymocytes reactive to systemically expressed self-antigens (Sha et al., 1988) might be affected by *Xcl1* deficiency. We found that the deletion of 2C-TCR$^+$CD4$^+$CD8$^+$ thymocytes in negatively selecting H-2$^{k/d}$ mice appeared undisturbed in the absence of XCL1 (Fig. 4 B). We further analyzed the role of XCL1 in the negative selection of thymocytes reactive to tissue-restricted antigens that are promiscuously expressed by mTECs. tDCs are known to cooperate with mTECs in the negative selection of thymocytes reactive to tissue-restricted antigens (Gallegos and Bevan, 2004). The rat insulin promoter (RIP)–driven transgene of membrane-bound OVA (mOVA) is expressed in the thymus by mTECs and deletes OVA-reactive OT-I-TCR and OT-II-TCR–transgenic thymocytes (Kurts et al., 1996). We found in irradiation-induced bone marrow chimera experiments that both OT-I-TCR–transgenic CD4$^-$CD8$^+$ and OT-II-TCR–transgenic CD4$^+$CD8$^-$ thymocytes were deleted in the thymic microenvironments of RIP-mOVA–transgenic mice even in the absence of XCL1 (Fig. 4 C), indicating that XCL1 is not needed for the negative selection of thymocytes reactive to the tissue-restricted antigen. These results collectively suggest that the role of XCL1 in negative selection is minor and dispensable.

Defective generation of nT reg cells in *Xcl1*-deficient mice

It was also shown that tDCs play a role in the thymic generation of nT reg cells (Watanabe et al., 2005; Proietto et al., 2008; Hanabuchi et al., 2010). We thus examined whether the generation of nT reg cells in the thymus might be affected in *Xcl1*-deficient mice. We found that CD4$^+$CD8$^-$CD25$^+$Foxp3$^+$

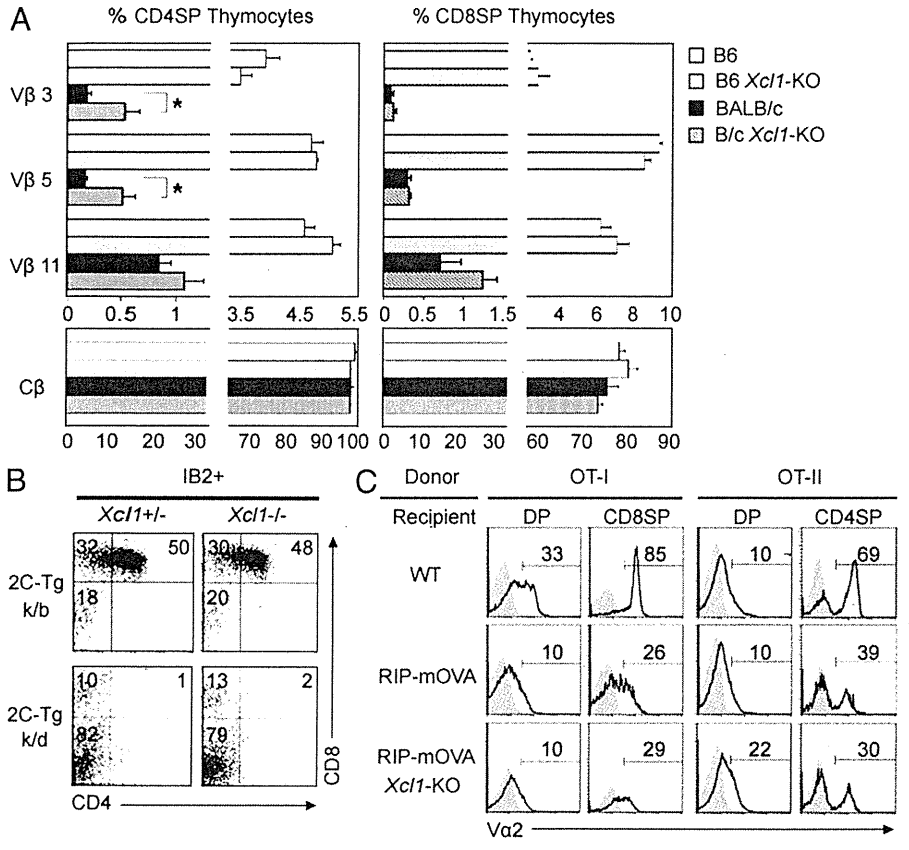

Figure 4. Negative selection of thymocytes in *Xcl1*-deficient mice. (A) Thymocytes isolated from WT and *Xcl1*-deficient (*Xcl1*-KO) mice of C57BL/6 and BALB/c backgrounds were three-color stained for CD4, CD8, and indicated TCR-Vβs. Monoclonal antibodies specific for Cβ, Vβ3, Vβ5, and Vβ11 used were H57-597, KJ25, MR9-4, and KT11, respectively. Shown are the means and standard errors of the frequencies of indicated $V\beta^{high}$ cells within $CD4^+CD8^-$ and $CD4^-CD8^+$ thymocytes from three independent measurements. *, $P < 0.05$. (B) Thymocytes from indicated mouse strains were three-color stained for CD4, CD8, and 2C-TCR (clone 1B2). Shown are the representative profiles of 2C-TCR–expressing cells from three independent experiments. (C) T cell–depleted bone marrow cells from OT-I-TCR-transgenic mice (left) or OT-II-TCR-transgenic mice (right) were transferred into lethally irradiated WT, RIP-mOVA-transgenic (RIP-mOVA), or RIP-mOVA-transgenic *Xcl1*-deficient (RIP-mOVA *Xcl1*-KO) H-2^b mice. Indicated thymocyte populations ($CD4^+CD8^+$, DP; $CD4^+CD8^-$, CD4SP; and $CD4^-CD8^+$, CD8SP) were stained for TCR-Vα2 (solid lines). Shaded profiles represent the analysis with control antibodies. Numbers indicate the frequency of $V\alpha2^{high}$ cells within indicated populations. Representative results of three independent experiments are shown.

T reg cells in the thymus of *Xcl1*-deficient adult mice showed reductions in frequency, as well as in absolute number, when compared with those in the thymus of WT mice (Fig. 5, A and B). The absolute numbers of thymic nT reg cells were significantly ($P < 0.05$) reduced in *Xcl1*-deficient mice throughout ontogeny from the day of birth to 3 mo old (Fig. 5 B). In contrast, the absolute numbers of other populations of thymocytes, including $CD4^-CD8^-$ double-negative, $CD4^+CD8^+$ double-positive, $CD4^+CD8^-$ CD4-single-positive, and $CD4^-CD8^+$ CD8-single-positive thymocytes, were comparable between *Xcl1*-deficient mice and WT mice (Fig. S4 A), indicating that the cell number reduction in the thymus of *Xcl1*-deficient mice was specific for thymic nT reg cells. A majority of $Foxp3^+$ nT reg cells in the thymus were localized in the medullary region (Fontenot et al., 2005; also shown in Fig. 5, C and D). The numbers per unit area of $Foxp3^+$ cells in the middle medullary M region, as well as the peripheral medullary CMJ-M region, were significantly ($P < 0.001$) smaller in *Xcl1*-deficient mice than in WT mice (Fig. 5, C and D). Among $Foxp3^+$ cells in the M and CMJ-M regions, the frequency of $CD11c^+$ DC-attached $Foxp3^+$ cells was severely reduced in *Xcl1*-deficient mice (Fig. 5, E and F), suggesting the role of tDCs in the XCL1-mediated regulation of nT reg cell generation in the thymus. $CD4^+CD8^-CD25^+$ cells isolated from the thymus of *Xcl1*-deficient mice and WT mice comparably suppressed the anti-CD3–stimulated proliferation of $CD4^+CD8^-CD25^-$ conventional T cells (Fig. 5 G), indicating that nT reg cells generated in the thymus of *Xcl1*-deficient mice are functional on a per cell basis but are defective in cell number. These results indicate that XCL1 is needed for the optimal generation of thymic nT reg cells.

Unlike the reduced number of nT reg cells in the thymus, the number of total $Foxp3^+$ cells in the periphery was not reduced in *Xcl1*-deficient mice throughout ontogeny (Fig. S4, B–D). However, the number of thymic nT reg cell–derived spleen nT reg cells, which were identified by the expression of the nuclear factor Helios along with Foxp3 (Sugimoto et al., 2006; Thornton et al., 2010), was reduced in *Xcl1*-deficient mice (Fig. 5 H and Fig. S4 E), suggesting that XCL1 deficiency causes the reduction of nT reg cells in the periphery.

No signs of tissue inflammation were detected in *Xcl1*-deficient mice at 6 wk old and 3 mo old (unpublished data). However, we detected inflammatory lesions and autoantibody deposits in several tissues, including heart, liver, stomach, salivary glands, and lacrimal glands, in *Xcl1*-deficient mice at 12–18 mo old (unpublished data). Importantly, the intravenous transfer of thymocytes from *Xcl1*-deficient BALB/c background mice into athymic BALB/c-*nu/nu* mice caused severe lymphocyte infiltration and tissue damage of lacrimal glands (Fig. 6, A and B). The tissue lesions were prominent in lacrimal glands, weakly detectable in salivary glands, and not detected in heart, liver, stomach, pancreas, or kidney. The administration of equal numbers of WT BALB/c thymocytes along with thymocytes from *Xcl1*-deficient mice significantly reduced the lesions in

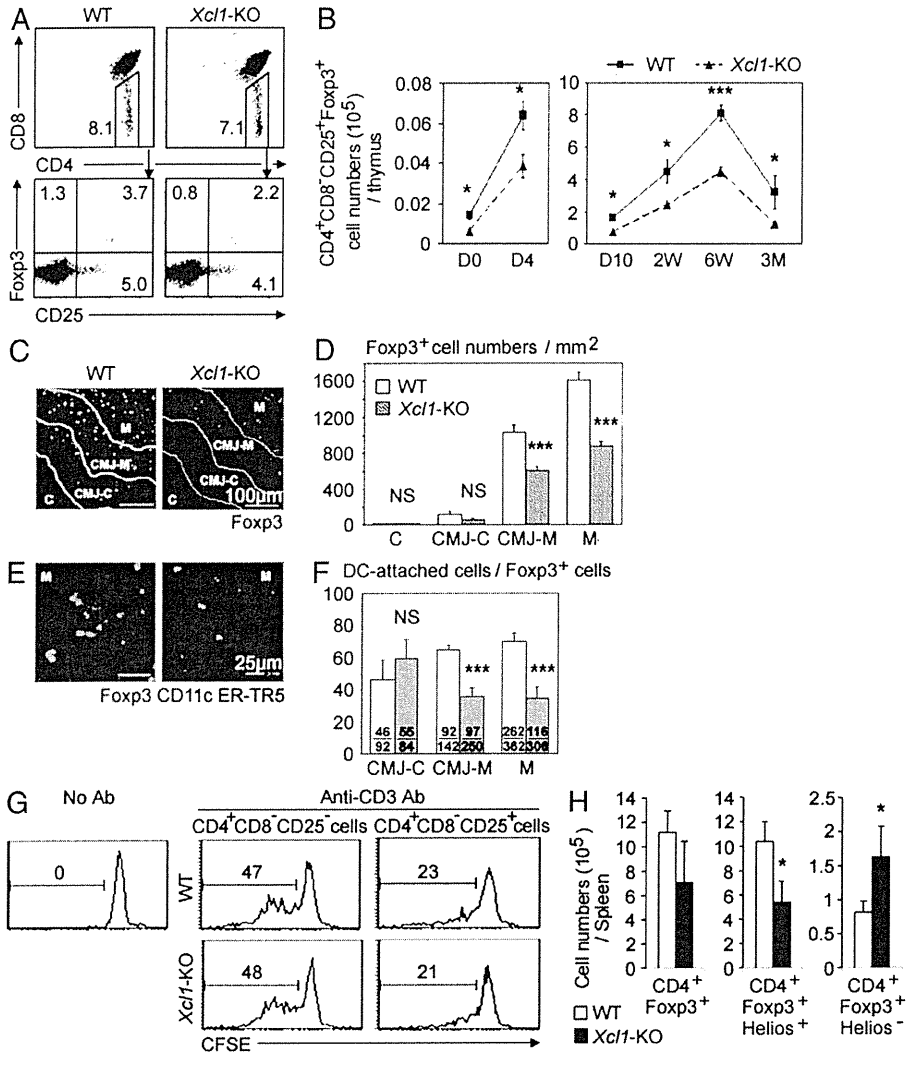

Figure 5. nT reg cell development in *Xcl1*-deficient mice. (A) Thymocytes from indicated mouse strains were four-color stained for CD4, CD8, CD25, and intracellular Foxp3. Numbers indicate the frequency of cells within indicated areas. Shown are the representative results of four independent experiments. (B) Means and standard errors ($n = 3$–11) of the absolute numbers of $CD4^+CD8^-CD25^+Foxp3^+$ thymocytes in indicated mice at indicated ages. (C) Immunofluorescence analysis of thymus sections from indicated mice for Foxp3. Letters and lines indicate the regions identified as in Fig. S2 A. (D) Numbers of $Foxp3^+$ thymocytes per unit area (1 mm^2) of the indicated regions. Means and standard errors of cell numbers from three independent measurements are shown. (E) Immunofluorescence analysis of thymus sections from indicated mice for Foxp3 (green), CD11c (red), and mTECs (ER-TR5; blue). Magnified images in the M region are shown. (F) Frequency (percentage) of $CD11c^+$ cell-attached cells among $Foxp3^+$ cells in indicated thymic regions. Means and standard errors of the frequencies from eight different images (bars) and the numbers of $CD11c^+$ cell-attached $Foxp3^+$ cells (top) and total $Foxp3^+$ cells (bottom) counted are shown. (G) Representative CFSE fluorescence profiles of $CD4^+CD25^-$ lymph node T cells from B6-Ly5.1 mice cultured in the absence or presence of $CD4^+CD8^-CD25^-$ or $CD4^+CD8^-CD25^+$ thymocytes from WT B6 (top) or *Xcl1*-deficient B6 background mice (bottom) with or without anti-CD3 antibody. Numbers indicate the frequency of $CFSE^{low}$ cells. Representative results of three independent experiments are shown. (H) Intracellular Helios and Foxp3 expression of $CD4^+$ spleen cells from WT and *Xcl1*-KO mice was analyzed by flow cytometry. Shown are the means and standard errors ($n = 3$) of cell numbers of $Foxp3^+$, $Foxp3^+Helios^+$, and $Foxp3^+Helios^-$ $CD4^+$ spleen cells from WT and *Xcl1*-KO mice. *, $P < 0.05$; ***, $P < 0.001$. NS, not significant ($P > 0.05$).

lacrimal glands (Fig. 6, A and B), suggesting that nT reg cells generated in the normal thymus are capable of suppressing the dacryoadenitis that nT reg cells generated in the thymus of *Xcl1*-deficient mice fail to control. These results indicate that nT reg cell development is impaired in the thymus of *Xcl1*-deficient mice and that the thymocytes from *Xcl1*-deficient mice are potent in causing, and fail to regulate, autoimmune dacryoadenitis.

Aire regulates medullary tDC localization and thymic nT reg cell generation

It was previously shown that $Aire^+$ mTECs play a role in the thymic generation of T reg cells (Aschenbrenner et al., 2007). Finally, we wished to examine whether the expression of Aire might be affected in the thymus of *Xcl1*-deficient mice and whether the expression of XCL1 might be affected in the thymus of *Aire*-deficient mice. The density of $Aire^+$ cells in the thymic medulla was comparable between *Xcl1*-deficient mice and WT mice (Fig. S4, F and G). Quantitative PCR analysis showed that the expression of *Aire* and Aire-dependent tissue-restricted antigens, such as *salivary protein 1*, was not diminished in mTECs isolated from *Xcl1*-deficient mice (unpublished data), indicating that XCL1 is not needed for the expression and function of Aire in mTECs.

In contrast, we found that the expression of *Xcl1* transcripts was severely defective in mTECs that were isolated from *Aire*-deficient mice (Fig. 7 A). As has been recently reported (Laan et al., 2009), the expression of other chemokines, such as *Ccl19*, *Ccl21*, and *Ccl25*, in mTECs was also modulated by the *Aire* deficiency (Fig. 7 A). However, the reduction of *Xcl1* in *Aire*-deficient mTECs was remarkably severe (the expression of which reduced to ~1% of that observed in normal mTECs), which is in contrast to the relatively mild alterations in the expression of the other chemokines in *Aire*-deficient mTECs (15–200% of the amount in normal mTECs; Fig. 7 A).

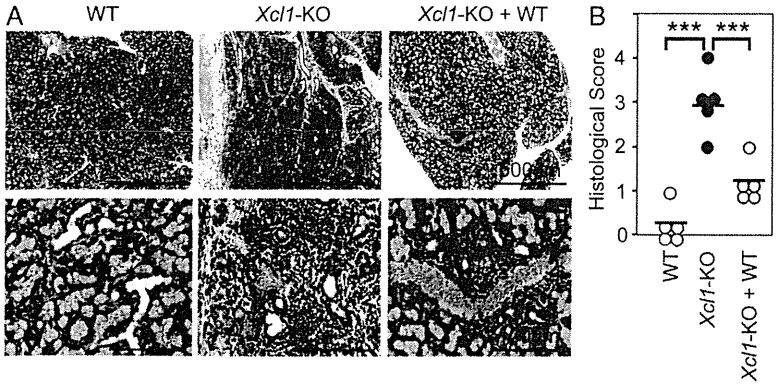

Figure 6. Thymocytes from *Xcl1*-deficient mice elicit inflammatory lesions in lacrimal glands in *nude* mice. 5×10^7 thymocytes isolated from WT or *Xcl1*-deficient (*Xcl1*-KO) mice of BALB/c background were intravenously transferred into BALB/c-*nu*/*nu* mice. Where indicated, equal numbers of thymocytes ($5 \times 10^7 + 5 \times 10^7$) were mixed before the transfer. Paraffin-embedded sections of lacrimal glands at 8 wk after the transfer were stained with hematoxylin and eosin. (A) Representative images of the sections at two different magnifications. (B) Histological scores of inflammatory lesions in the lacrimal glands ($n = 5$). Horizontal bars indicate the means. ***, $P < 0.001$.

The density of tDCs in the middle medullary M region was significantly ($P < 0.01$) decreased in *Aire*-deficient mice, whereas that in the CMJ-C region was significantly ($P < 0.05$) elevated in *Aire*-deficient mice (Fig. 7, B and C). The density of tDCs in the other regions (SCZ, C, and CMJ-M regions) was not significantly ($P > 0.05$) altered by the *Aire* deficiency (Fig. 7, B and C). The absolute numbers of tDCs and their subsets were not affected in *Aire*-deficient mice (Fig. 7 D). These results indicate that as in *Xcl1*-deficient mice, *Aire*-deficient mice exhibit defective accumulation of tDCs in the medullary region.

The density of Foxp3$^+$ cells in the thymic medulla (CMJ-M and M regions) was accordingly and significantly ($P < 0.05$) lower in *Aire*-deficient mice than in WT mice (Fig. 7, E and F). Moreover, the absolute number of CD4$^+$CD8$^-$CD25$^+$Foxp3$^+$ cells in the thymus was significantly ($P < 0.05$) reduced in *Aire*-deficient mice (Fig. 7 G). These results indicate that *Aire*-deficient mice exhibit defective generation of nT reg cells in the thymus.

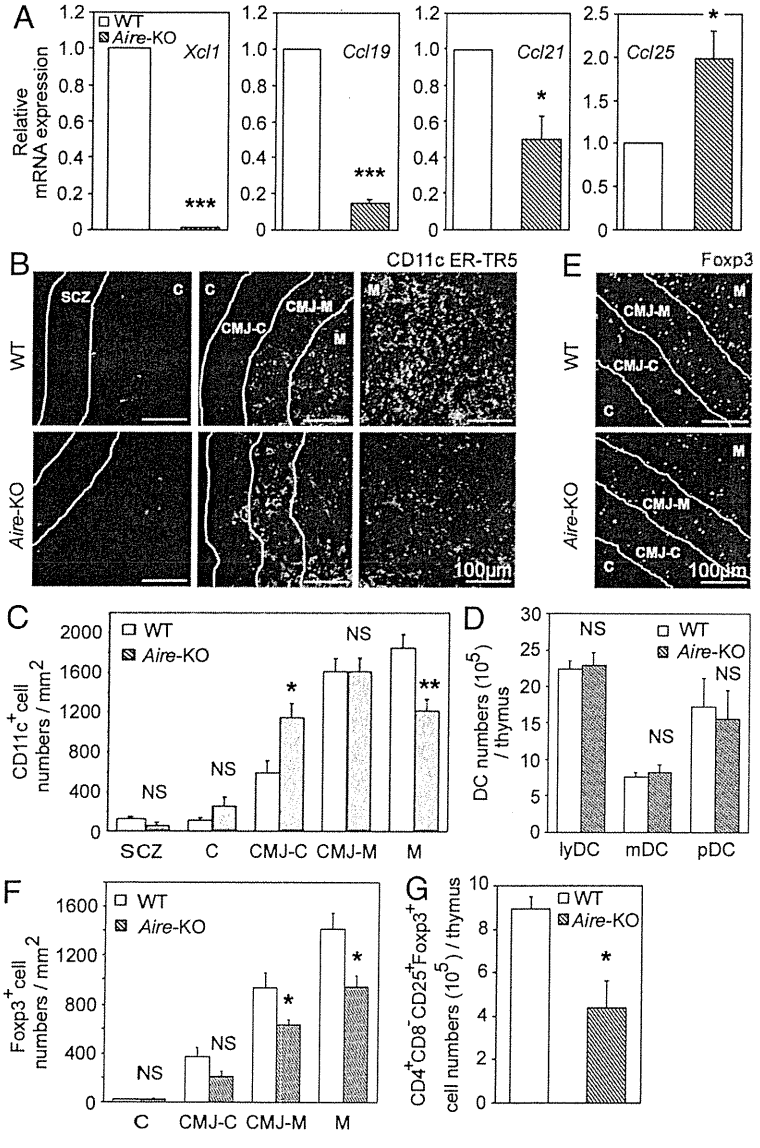

Figure 7. DCs and T reg cells in the thymus of *Aire*-deficient mice. (A) Quantitative RT-PCR analysis of *Xcl1*, *Ccl19*, *Ccl21*, and *Ccl25* expression in sorted CD45$^-$EpCAM$^+$UEA1$^+$ mTECs from WT and *Aire*-deficient mice. The amounts of the transcripts were normalized to the amount of housekeeping *Hprt*, and those in WT mTECs were arbitrarily set to 1. Bar graphs show means and standard errors of at least three independent measurements. (B) Immunofluorescence analysis of thymus sections for CD11c (green) and mTECs (ER-TR5; red). Representative images from two independent experiments are shown. Lines indicate borders among the indicated regions identified as in Fig. S2 A. (C) Numbers of CD11c$^+$ cells per unit area (1 mm^2) of the indicated regions were measured. Means and standard errors of cell numbers are shown. (D) Means and standard errors ($n = 3$–4) of the absolute numbers of indicated DC subpopulations in the thymus of indicated mouse strains are shown. (E) Immunofluorescence analysis of thymus sections from indicated mice for Foxp3. Representative images from two independent experiments are shown. (F) Numbers of Foxp3$^+$ cells per unit area (1 mm^2) of the indicated areas were measured. Means and standard errors of cell numbers from three independent measurements are shown. (G) Means and standard errors ($n = 3$) of the absolute numbers of CD4$^+$CD8$^-$CD25$^+$Foxp3$^+$ cells in the thymus of indicated mice. *, $P < 0.05$; **, $P < 0.01$; ***, $P < 0.001$. NS, not significant ($P > 0.05$).

DISCUSSION

It is well known that tDCs are detected abundantly in the medullary region and sparsely in the cortical region (Barclay and Mayrhofer, 1981; Flotte et al., 1983; Kurobe et al., 2006). However, the molecular mechanisms that contribute to this medullary accumulation of tDCs are unknown. Screening for the chemokine receptors expressed by tDCs and their chemotactic responses to candidate ligands has revealed that the chemokine ligands for CCR7, CXCR4, and XCR1 are capable of attracting tDCs. By analyzing mice deficient for these chemokine ligands or their receptors, we identify that the XCL1–XCR1 chemokine axis plays a potent role in the medullary accumulation of tDCs. In contrast, we find that CCR7 and CXCR4 play a minor, if any, role in the accumulation of tDCs in the thymic medulla.

XCL1, which is also known as lymphotactin, ATAC, and SCM1, is the only member of the C family of chemokines encoded in the mouse genome (Kelner et al., 1994). XCL1 is produced by activated $CD8^+$ T cells, Th1-polarized $CD4^+$ T cells, and NK cells (Kelner et al., 1994; Hedrick et al., 1997; Dorner et al., 2002, 2004, 2009). A recent study shows that the XCL1 receptor, XCR1, is expressed by $CD8^+$ DCs in the spleen and that the XCL1-XCR1–mediated interaction between $CD8^+$ T cells and $CD8^+$ DCs is important for the development of cytotoxicity of $CD8^+$ T cells to antigens cross-presented by $CD8^+$ DCs (Dorner et al., 2009). However, the functions of the XCL1–XCR1 chemokine axis in the thymus have remained unknown. This study reveals the role of the XCL1–XCR1 chemokine axis in the localization of tDCs in the thymic medulla.

In the thymus, XCR1 is exclusively expressed by tDCs. Among the tDC subpopulations, XCR1 is most highly detectable in I-$A^{high}CD11c^{high}CD11b^-$ lymphoid DCs, a population that largely overlaps with the $CD8^+Sirp\alpha^-$ conventional DC subpopulation of tDCs (Wu and Shortman, 2005). In contrast, XCL1 in the thymus is expressed in the class II MHC^{high} subpopulation of mTECs in addition to NK and NKT cells. The *Xcl1* transcripts expressed by mTECs are in smaller amounts than those expressed by activated $CD8^+$ T cells in the spleen but are prominent in the thymus when compared with those expressed by other cells in the thymus, including cTECs, thymic fibroblasts, tDCs, or $CD45^+$ thymocytes. In *Xcl1*-deficient mice, tDCs fail to localize in the medullary region and are instead accumulated in the deep cortex and CMJ regions, although the numbers and subpopulations of tDCs are not altered. The mislocalization of tDCs in the deep cortex and CMJ regions of the thymus was detected in irradiated *Xcl1*-deficient mice that were reconstituted with normal bone marrow cells but not in irradiated normal mice that were reconstituted with *Xcl1*-deficient bone marrow cells (unpublished data). These results suggest that XCL1 produced by irradiation-resistant thymic stromal cells, rather than irradiation-sensitive bone marrow–derived thymocytes, contributes to the attraction of XCR1-expressing tDCs into the inner medullary region of the thymus. We think that mTECs, rather than hematopoietic cells including NK cells and NKT cells, in the thymus play a major role in the XCL1-mediated medullary localization of tDCs.

The arrest of tDCs in the deep cortex and CMJ regions in *Xcl1*-deficient mice suggests that the tDCs that are accumulated in the medullary region of normal mice may be derived from tDCs that are either generated in the deep cortex and CMJ regions of the thymus or migrate into the thymus from the circulation at the deep cortex and CMJ regions. The XCL1-mediated attraction of XCR1-expressing tDCs to the medulla may facilitate efficient interactions between mTECs and tDCs. It is also possible that the distribution of tDCs may be further regulated by the balance between the XCL1-mediated attraction to the medullary region and the attraction to the deep cortex and CMJ regions by unknown factors, and the loss of XCL1 may result in the aberrant attraction of tDCs to the deep cortex and CMJ regions.

Our results also reveal that Aire is essential for the production of XCL1 by mTECs. Aire is a nuclear factor expressed by a subpopulation of mTECs and is implicated for its role in the promiscuous gene expression of tissue-restricted self-antigens in mTECs (Derbinski et al., 2005; Mathis and Benoist, 2009). It is also suggested that Aire regulates the development of mTECs, thereby indirectly contributing to the promiscuous gene expression in mTECs (Gillard et al., 2007; Yano et al., 2008). Our results show that the expression of *Xcl1* transcripts in mTECs isolated from *Aire*-deficient mice is severely reduced to ~1% of the amount observed in WT mTECs. Accordingly, as in *Xcl1*-deficient mice, the medullary accumulation of tDCs is severely impaired in *Aire*-deficient mice and the tDCs are aberrantly arrested in the deep cortex and CMJ regions. Aire may regulate the development of XCL1-producing mTECs. Alternatively, Aire may promiscuously regulate the expression of *Xcl1* gene in mTECs.

Concomitant with the failure in the medullary accumulation of tDCs, mice deficient for either *Xcl1* or *Aire* exhibit a reduction in the number of T reg cells generated in the thymus. Most T reg cells in the thymus are generated in the medullary region (Fontenot et al., 2005) and it is suggested that mTECs (Aschenbrenner et al., 2007; Spence and Green, 2008), tDCs (Proietto et al., 2008; Hanabuchi et al., 2010), and their cooperation (Watanabe et al., 2005) contribute to the generation of T reg cells in the thymus. Our results indicate that the deficiency of either *Xcl1* or *Aire* causes the reduced generation of T reg cells in the thymus. The cellularity of thymic T reg cells in *Xcl1*-deficient mice and *Aire*-deficient mice is approximately half of that in WT mice and is significantly low when compared with that in WT mice. However, the reduced numbers of thymic T reg cells are not significantly ($P > 0.05$) different between *Xcl1*-deficient mice and *Aire*-deficient mice. Our results also indicate that *Aire* deficiency causes severe loss of XCL1 expression by mTECs, whereas *Xcl1* deficiency does not reduce Aire expression by mTECs. We therefore think that Aire is essential for the mTEC expression of XCL1, which attracts XCR1-expressing tDCs to the medullary region and contributes to the optimal generation of T reg cells in the thymus.

Proximal interactions between tDCs and mTECs in the thymic medulla may promote optimal generation of nT reg cells, possibly via the production of γc cytokines, including IL-2, IL-7, and thymic stromal lymphopoietin (Watanabe et al., 2005; Ziegler and Liu, 2006; Mazzucchelli et al., 2008; Vang et al., 2008). Among the tDC subpopulations, lymphoid DCs most highly express XCR1 and, thus, may play a major role in the interaction with mTECs and the generation of nT reg cells. Unlike tDCs, $CD4^+CD8^-CD25^+$ thymic T reg cells do not express detectable *Xcr1* transcripts (unpublished data), ruling out the possibility of a direct effect of XCL1 on T reg cells. Thus, our results suggest that XCL1-producing mTECs attract tDCs into the inner medullary region, thereby promoting the generation of nT reg cells, and that optimal nT reg cell development in the thymus requires a specialized medullary microenvironment that is formed by the XCL1-mediated attraction of tDCs by Aire-dependent mTECs. Whether XCL1-mediated tDC accumulation in the medulla affects TCR repertoire of nT reg cells remains unclear.

A recent work using CD11c-Cre mice crossed with mice that express diphtheria toxin A under the control of a loxP-flanked neomycin resistance cassette from the ROSA26 locus has shown that these DC-depleted mice are not defective in the generation of nT reg cells in the thymus (Ohnmacht et al., 2009), potentially contradicting our results indicating the role of tDCs in nT reg cell generation. However, that work also described that the depletion of tDCs is incomplete in the DC-depleted mice (Ohnmacht et al., 2009) but did not describe the intrathymic localization of the remaining tDCs. Thus, the incompletely depleted tDCs in the DC-depleted mice may be enriched in the inner medullary region and be sufficient for the unreduced generation of nT reg cells.

Our results show that the number of nT reg cells in the thymus is reduced in *Aire*-deficient mice. However, several studies have described that the generation of T reg cells is not defective in *Aire*-deficient mice (Anderson et al., 2002, 2005; Liston et al., 2003; Kuroda et al., 2005; Hubert et al., 2009), particularly in the spleen and the lymph nodes (Anderson et al., 2005; Kuroda et al., 2005; Hubert et al., 2009). Indeed, our results show that the number of T reg cells in *Aire*-deficient mice is reduced in the thymus to approximately half of that in WT mice but is not reduced in the spleen and the lymph nodes of *Aire*-deficient mice. It should be noted that previous studies have indicated that the number of T reg cells in the thymus is slightly reduced in *Aire*-deficient mice, although those studies concluded no loss of T reg cell generation in the thymus (Anderson et al., 2005; Kuroda et al., 2005; Hubert et al., 2009). We think that Aire indeed contributes to the optimal generation of nT reg cells in the thymus and that the generation of induced T reg cells, particularly in the periphery (Piccirillo and Shevach, 2004; Curotto de Lafaille and Lafaille, 2009), has veiled the reduced cellularity of nT reg cells in *Aire*-deficient mice.

The present results show that thymocytes from *Xcl1*-deficient mice are potent in eliciting severe lymphocyte infiltration and tissue damage of lacrimal glands in athymic *nu/nu* mice, indicating that the thymocytes generated in *Xcl1*-deficient mice fail to establish self-tolerance. The mixture of thymocytes from normal mice reduces the dacryoadenitis caused by the thymocytes from *Xcl1*-deficient mice, supporting the possibility that the thymocytes from *Xcl1*-deficient mice are potent in triggering, and fail to regulate, the autoimmunity and that nT reg cell development is impaired in the thymus of *Xcl1*-deficient mice. In a similar manner, *Aire*-deficient mice tend to exhibit inflammatory failure of exocrine tissues, including lacrimal glands (Anderson et al., 2002, 2005; Kuroda et al., 2005; Hubert et al., 2009). The commonness of the target organs may reflect a similarity in the breakdown of self-tolerance in *Xcl1*-deficient mice and *Aire*-deficient mice. Nonetheless, our results do not rule out the possibility that the absence of XCL1 in peripheral T cells also contributes to the onset of the dacryoadenitis.

Finally, our results reveal that the XCL1-mediated medullary accumulation of tDCs plays only a minor role in the negative selection of self-reactive thymocytes. In contrast, tDCs are known for their roles in negative selection, particularly in the intrathymic presentation of peripheral antigens, by cooperating with promiscuous gene expression in mTECs (Gallegos and Bevan, 2004; Koble and Kyewski, 2009; Nitta et al., 2009) and by transport from the circulation (Bonasio et al., 2006). The tDCs that are mislocalized in the CMJ regions in the absence of XCL1 may be sufficient for the cross-presentation of mTEC-expressed tissue-restricted antigens and the negative selection of developing thymocytes reactive to those self-antigens. In addition, recent studies indicated that DCs in the thymic cortex are capable of inducing the deletion of negatively selected thymocytes (McCaughtry et al., 2008) and that CCR2 is involved in the accumulation of $CD8^-Sirp\alpha^+$ tDC subpopulation in the thymic cortex and the intrathymic negative selection against blood-borne antigens (Baba et al., 2009). Thus, the XCL1-mediated medullary accumulation is not needed for the deletion of the majority of negatively selected thymocytes.

In conclusion, the present results indicate that the XCL1–XCR1 chemokine axis contributes to the medullary accumulation of tDCs and the thymic development of nT reg cells. The results also suggest that Aire expressed in mTECs regulates the XCL1-mediated medullary accumulation of tDCs and that XCL1-mediated proximal interaction between tDCs and mTECs in the thymic medulla contributes to the thymic development of nT reg cells. Our results imply a novel role of Aire in regulating autoimmunity via the XCL1-mediated medullary accumulation of tDCs and that the breakdown of self-tolerance in Aire deficiency may involve the failure to localize tDCs in the medulla in an XCL1-dependent manner.

MATERIALS AND METHODS

Mice. *Xcl1*-deficient mice were generated at Merck Research Laboratories (Fig. S1, A–C). *Aire*-deficient mice were generated at the University of Basel (Fig. S5). *Ccr7*-deficient mice (Förster et al., 1999), Mx-Cre x $Cxcr4^{flox/flox}$ mice (Sugiyama et al., 2006), and *plt/plt* mice (Nakano et al., 1998), as well as OT-I and OT-II TCR-transgenic and RIP-mOVA–transgenic mice (Kurts et al., 1996; Barnden et al., 1998), were described previously. Mx-Cre x $Cxcr4^{flox/flox}$ mice were injected with poly I poly C, and only mice that

exhibited a nearly complete loss of CXCR4 genomic sequence and the undetectable expression of CXCR4 gene in hematopoietic cells were further analyzed (Sugiyama et al., 2006). Mice were maintained under specific pathogen-free conditions in our animal facility, and experiments were performed under the approval of the Institutional Animal Care Committee of the University of Tokushima.

Bone marrow chimeras. Bone marrow cells were magnetically depleted of T cells using biotin-conjugated antibodies specific for CD4, CD8, and Thy1.2 and streptavidin-conjugated magnetic beads (Miltenyi Biotec). Recipient mice were injected with T cell–depleted bone marrow cells (4×10^7) 1 d after 9.25 Gy x-ray irradiation. The mice were analyzed 4–5 wk after the reconstitution.

Thymocyte transfer into *nude* mice. 5×10^7 thymocytes isolated from WT or *Xcl1*-deficient (*Xcl1*-KO) mice of BALB/c background were intravenously transferred into BALB/c-*nu*/*nu* mice. Where indicated, equal numbers of thymocytes ($5 \times 10^7 + 5 \times 10^7$) were mixed before the transfer. Various organs at 8 wk after the transfer were fixed with 4% phosphate-buffered formaldehyde, pH 7.2. Paraffin-embedded sections were stained with hematoxylin and eosin. Two pathologists independently evaluated the histology without being informed of the conditions of individual mice. Inflammatory lesions of the tissues were scored as previously described (Ishimaru et al., 2008) and as follows: 0 = no inflammation, 1 = 1–5 foci composed of >20 mononuclear cells per focus, 2 = >5 such foci but without significant parenchymal destruction, 3 = degeneration of parenchymal tissue, and 4 = extensive infiltration with mononuclear cells and extensive parenchymal destruction.

Flow cytometry analysis. Multicolor flow cytometry analysis and cell sorting were performed using FACSCalibur and FACSAria II (BD). Intracellular staining of Foxp3 and Helios was performed according to the manufacturer's instructions (eBioscience). Thymic stromal cells were prepared by digesting thymic fragments with collagenase, dispase, and DNase I (Roche) and enriched by depleting $CD45^+$ cells with a magnetic cell sorter (Miltenyi Biotec) before cell sorting, as described previously (Gray et al., 2002). For DC analysis, thymus cells were prepared by digesting thymic fragments with collagenase D and DNase I.

Immunofluorescence analysis. Frozen thymus tissues embedded in OCT compound (Sakura) were sliced into 5-µm-thick sections, fixed with acetone, and stained with the following antibodies: mTEC-specific monoclonal antibody ER-TR5 (a gift from W. van Ewijk, Erasmus University, Rotterdam, Netherlands) followed by Alexa Fluor 633–conjugated anti–rat IgG antibody (Invitrogen); biotinylated UEA1 (Vector Laboratories) followed by Alexa Fluor 633–conjugated streptavidin (Invitrogen); FITC-conjugated anti-Foxp3 monoclonal antibody (eBioscience); biotinylated anti-CD11c or anti-CD11b monoclonal antibody (eBioscience) followed by Alexa Fluor 488–conjugated or Alexa Fluor 546–conjugated streptavidin (Invitrogen); and anti-Aire antibody (Santa Cruz Biotechnology, Inc.) followed by FITC-conjugated anti–rabbit IgG antibody (Invitrogen). Images were analyzed with a TSC SP2 confocal laser-scanning microscope and Confocal software version 2.6 (Leica).

Chemotaxis assay. 10^6 collagenase-digested thymus cells were placed in a Transwell chamber (6.5-mm diameter, 5-µm pore; Corning) that was inserted into a 100-nM chemokine-containing culture well. Cells were incubated for 2 h, counted, stained for CD11c and $I\text{-}A^b$, and analyzed by flow cytometry. Chemotactic index is the ratio of the numbers of $CD11c^+I\text{-}A^{b+}$ DCs that migrated to the bottom of culture wells in the presence and absence of chemokines.

Measurement of T reg cell function. According to the methods previously reported (Tai et al., 2005), 5×10^4 CFSE-labeled $CD4^+CD25^-$ lymph node T cells isolated from B6-Ly5.1 mice were cultured with 5×10^4 $CD25^+CD4^+CD8^-$ or $CD25^-CD4^+CD8^-$ thymocytes in the presence of 10^5 20 Gy-irradiated T cell–depleted spleen cells from B6 mice and 1 µg/ml anti-CD3 monoclonal antibody (clone 2C11). Cells were harvested at 72 h and analyzed by flow cytometry.

RT-PCR analysis. Total cellular RNA was reverse transcribed with oligo-dT primer and Superscript III reverse transcription (Invitrogen). cDNA was PCR amplified, electrophoresed, and visualized with ethidium bromide. For quantitative analysis, real-time RT-PCR was performed using SYBR Premix Ex Taq (Takara Bio Inc.) and Light Cycler DX400 (Roche). Amplified products were confirmed to be single bands by gel electrophoresis and were normalized to the amount of HPRT products. Primer sequences are listed in Table S1.

Statistical analysis. Statistical comparison was performed with the Student's *t* test (two-tailed) using Excel software (Microsoft).

Online supplemental material. Fig. S1 shows genomic structure of *Xcl1*-deficient mice. Fig. S2 shows analysis of $CD11c^+$ cells in thymus sections. Fig. S3 shows negative selection of T cells in the periphery of *Xcl1*-deficient mice. Fig. S4 shows thymocytes, splenocytes, and $Aire^+$ mTECs in *Xcl1*-deficient mice. Fig. S5 shows targeting strategy to generate *Aire*-Cre-GFP knockin mice. Table S1 shows primer sequences used for RT-PCR analysis. Online supplemental material is available at http://www.jem.org/cgi/content/full/jem.20102327/DC1.

We would like to express our special appreciation to the late professor Cunlan Liu for initiating the present study. We also would like to thank Tomoo Ueno and Fumi Saito for technical support in the laboratory and Kensuke Takada for reading the manuscript.

This study was supported by a MEXT Grant-in-Aid for Scientific Research on Priority Area "Immunological Self", the JST Strategic International Cooperative Program, the Swiss National Science Foundation, the European Framework Programme 6, and the Max Planck Society.

The authors have no competing financial interests.

Submitted: 5 November 2010
Accepted: 12 January 2011

REFERENCES

Anderson, G., P.J. Lane, and E.J. Jenkinson. 2007. Generating intrathymic microenvironments to establish T-cell tolerance. *Nat. Rev. Immunol.* 7:954–963. doi:10.1038/nri2187

Anderson, M.S., E.S. Venanzi, L. Klein, Z. Chen, S.P. Berzins, S.J. Turley, H. von Boehmer, R. Bronson, A. Dierich, C. Benoist, and D. Mathis. 2002. Projection of an immunological self shadow within the thymus by the Aire protein. *Science.* 298:1395–1401. doi:10.1126/science.1075958

Anderson, M.S., E.S. Venanzi, Z. Chen, S.P. Berzins, C. Benoist, and D. Mathis. 2005. The cellular mechanism of Aire control of T cell tolerance. *Immunity.* 23:227–239. doi:10.1016/j.immuni.2005.07.005

Aschenbrenner, K., L.M. D'Cruz, E.H. Vollmann, M. Hinterberger, J. Emmerich, L.K. Swee, A. Rolink, and L. Klein. 2007. Selection of $Foxp3^+$ regulatory T cells specific for self antigen expressed and presented by $Aire^+$ medullary thymic epithelial cells. *Nat. Immunol.* 8:351–358. doi:10.1038/ni1444

Baba, T., Y. Nakamoto, and N. Mukaida. 2009. Crucial contribution of thymic Sirp α^+ conventional dendritic cells to central tolerance against blood-borne antigens in a CCR2-dependent manner. *J. Immunol.* 183:3053–3063. doi:10.4049/jimmunol.0900438

Barclay, A.N., and G. Mayrhofer. 1981. Bone marrow origin of Ia-positive cells in the medulla rat thymus. *J. Exp. Med.* 153:1666–1671. doi:10.1084/jem.153.6.1666

Barnden, M.J., J. Allison, W.R. Heath, and F.R. Carbone. 1998. Defective TCR expression in transgenic mice constructed using cDNA-based alpha- and beta-chain genes under the control of heterologous regulatory elements. *Immunol. Cell Biol.* 76:34–40. doi:10.1046/j.1440-1711.1998.00709.x

Bonasio, R., M.L. Scimone, P. Schaerli, N. Grabie, A.H. Lichtman, and U.H. von Andrian. 2006. Clonal deletion of thymocytes by circulating

dendritic cells homing to the thymus. *Nat. Immunol.* 7:1092–1100. doi:10.1038/ni1385

Curotto de Lafaille, M.A., and J.J. Lafaille. 2009. Natural and adaptive foxp3$^+$ regulatory T cells: more of the same or a division of labor? *Immunity.* 30:626–635. doi:10.1016/j.immuni.2009.05.002

Derbinski, J., A. Schulte, B. Kyewski, and L. Klein. 2001. Promiscuous gene expression in medullary thymic epithelial cells mirrors the peripheral self. *Nat. Immunol.* 2:1032–1039. doi:10.1038/ni723

Derbinski, J., J. Gäbler, B. Brors, S. Tierling, S. Jonnakuty, M. Hergenhahn, L. Peltonen, J. Walter, and B. Kyewski. 2005. Promiscuous gene expression in thymic epithelial cells is regulated at multiple levels. *J. Exp. Med.* 202:33–45. doi:10.1084/jem.20050471

Dorner, B.G., A. Scheffold, M.S. Rolph, M.B. Huser, S.H. Kaufmann, A. Radbruch, I.E. Flesch, and R.A. Kroczek. 2002. MIP-1α, MIP-1β, RANTES, and ATAC/lymphotactin function together with IFN-γ as type 1 cytokines. *Proc. Natl. Acad. Sci. USA.* 99:6181–6186. doi:10.1073/pnas.092141999

Dorner, B.G., H.R. Smith, A.R. French, S. Kim, J. Poursine-Laurent, D.L. Beckman, J.T. Pingel, R.A. Kroczek, and W.M. Yokoyama. 2004. Coordinate expression of cytokines and chemokines by NK cells during murine cytomegalovirus infection. *J. Immunol.* 172:3119–3131.

Dorner, B.G., M.B. Dorner, X. Zhou, C. Opitz, A. Mora, S. Güttler, A. Hutloff, H.W. Mages, K. Ranke, M. Schaefer, et al. 2009. Selective expression of the chemokine receptor XCR1 on cross-presenting dendritic cells determines cooperation with CD8$^+$ T cells. *Immunity.* 31:823–833. doi:10.1016/j.immuni.2009.08.027

Flotte, T.J., T.A. Springer, and G.J. Thorbecke. 1983. Dendritic cell and macrophage staining by monoclonal antibodies in tissue sections and epidermal sheets. *Am. J. Pathol.* 111:112–124.

Fontenot, J.D., J.P. Rasmussen, L.M. Williams, J.L. Dooley, A.G. Farr, and A.Y. Rudensky. 2005. Regulatory T cell lineage specification by the forkhead transcription factor foxp3. *Immunity.* 22:329–341. doi:10.1016/j.immuni.2005.01.016

Förster, R., A. Schubel, D. Breitfeld, E. Kremmer, I. Renner-Müller, E. Wolf, and M. Lipp. 1999. CCR7 coordinates the primary immune response by establishing functional microenvironments in secondary lymphoid organs. *Cell.* 99:23–33. doi:10.1016/S0092-8674(00)80059-8

Gallegos, A.M., and M.J. Bevan. 2004. Central tolerance to tissue-specific antigens mediated by direct and indirect antigen presentation. *J. Exp. Med.* 200:1039–1049. doi:10.1084/jem.20041457

Gillard, G.O., J. Dooley, M. Erickson, L. Peltonen, and A.G. Farr. 2007. Aire-dependent alterations in medullary thymic epithelium indicate a role for Aire in thymic epithelial differentiation. *J. Immunol.* 178:3007–3015.

Gray, D.H., A.P. Chidgey, and R.L. Boyd. 2002. Analysis of thymic stromal cell populations using flow cytometry. *J. Immunol. Methods.* 260:15–28. doi:10.1016/S0022-1759(01)00493-8

Hanabuchi, S., T. Ito, W.R. Park, N. Watanabe, J.L. Shaw, E. Roman, K. Arima, Y.H. Wang, K.S. Voo, W. Cao, and Y.J. Liu. 2010. Thymic stromal lymphopoietin-activated plasmacytoid dendritic cells induce the generation of FOXP3$^+$ regulatory T cells in human thymus. *J. Immunol.* 184:2999–3007. doi:10.4049/jimmunol.0804106

Hedrick, J.A., V. Saylor, D. Figueroa, L. Mizoue, Y. Xu, S. Menon, J. Abrams, T. Handel, and A. Zlotnik. 1997. Lymphotactin is produced by NK cells and attracts both NK cells and T cells in vivo. *J. Immunol.* 158:1533–1540.

Hubert, F.X., S.A. Kinkel, P.E. Crewther, P.Z. Cannon, K.E. Webster, M. Link, R. Uibo, M.K. O'Bryan, A. Meager, S.P. Forehan, et al. 2009. Aire-deficient C57BL/6 mice mimicking the common human 13-base pair deletion mutation present with only a mild autoimmune phenotype. *J. Immunol.* 182:3902–3918. doi:10.4049/jimmunol.0802124

Ishimaru, N., R. Arakaki, S. Yoshida, A. Yamada, S. Noji, and Y. Hayashi. 2008. Expression of the retinoblastoma protein RbAp48 in exocrine glands leads to Sjögren's syndrome-like autoimmune exocrinopathy. *J. Exp. Med.* 205:2915–2927. doi:10.1084/jem.20080174

Jenkinson, E.J., G. Anderson, and J.J. Owen. 1992. Studies on T cell maturation on defined thymic stromal cell populations in vitro. *J. Exp. Med.* 176:845–853. doi:10.1084/jem.176.3.845

Kelner, G.S., J. Kennedy, K.B. Bacon, S. Kleyensteuber, D.A. Largaespada, N.A. Jenkins, N.G. Copeland, J.F. Bazan, K.W. Moore, T.J. Schall, and A. Zlotnik. 1994. Lymphotactin: a cytokine that represents a new class of chemokine. *Science.* 266:1395–1399. doi:10.1126/science.7973732

Klein, L., M. Hinterberger, G. Wirnsberger, and B. Kyewski. 2009. Antigen presentation in the thymus for positive selection and central tolerance induction. *Nat. Rev. Immunol.* 9:833–844. doi:10.1038/nri2669

Koble, C., and B. Kyewski. 2009. The thymic medulla: a unique microenvironment for intercellular self-antigen transfer. *J. Exp. Med.* 206:1505–1513. doi:10.1084/jem.20082449

Kurobe, H., C. Liu, T. Ueno, F. Saito, I. Ohigashi, N. Seach, R. Arakaki, Y. Hayashi, T. Kitagawa, M. Lipp, et al. 2006. CCR7-dependent cortex-to-medulla migration of positively selected thymocytes is essential for establishing central tolerance. *Immunity.* 24:165–177. doi:10.1016/j.immuni.2005.12.011

Kuroda, N., T. Mitani, N. Takeda, N. Ishimaru, R. Arakaki, Y. Hayashi, Y. Bando, K. Izumi, T. Takahashi, T. Nomura, et al. 2005. Development of autoimmunity against transcriptionally unrepressed target antigen in the thymus of Aire-deficient mice. *J. Immunol.* 174:1862–1870.

Kurts, C., W.R. Heath, F.R. Carbone, J. Allison, J.F. Miller, and H. Kosaka. 1996. Constitutive class I–restricted exogenous presentation of self antigens in vivo. *J. Exp. Med.* 184:923–930. doi:10.1084/jem.184.3.923

Laan, M., K. Kisand, V. Kont, K. Möll, L. Tserel, H.S. Scott, and P. Peterson. 2009. Autoimmune regulator deficiency results in decreased expression of CCR4 and CCR7 ligands and in delayed migration of CD4$^+$ thymocytes. *J. Immunol.* 183:7682–7691. doi:10.4049/jimmunol.0804133

Liston, A., S. Lesage, J. Wilson, L. Peltonen, and C.C. Goodnow. 2003. Aire regulates negative selection of organ-specific T cells. *Nat. Immunol.* 4:350–354. doi:10.1038/ni906

Mathis, D., and C. Benoist. 2009. Aire. *Annu. Rev. Immunol.* 27:287–312. doi:10.1146/annurev.immunol.25.022106.141532

Mazzucchelli, R., J.A. Hixon, R. Spolski, X. Chen, W.Q. Li, V.L. Hall, J. Willette-Brown, A.A. Hurwitz, W.J. Leonard, and S.K. Durum. 2008. Development of regulatory T cells requires IL-7Ralpha stimulation by IL-7 or TSLP. *Blood.* 112:3283–3292. doi:10.1182/blood-2008-02-137414

McCaughtry, T.M., T.A. Baldwin, M.S. Wilken, and K.A. Hogquist. 2008. Clonal deletion of thymocytes can occur in the cortex with no involvement of the medulla. *J. Exp. Med.* 205:2575–2584. doi:10.1084/jem.20080866

Moore, N.C., G. Anderson, D.E. McLoughlin, J.J. Owen, and E.J. Jenkinson. 1994. Differential expression of Mtv loci in MHC class II-positive thymic stromal cells. *J. Immunol.* 152:4826–4831.

Nakano, H., S. Mori, H. Yonekawa, H. Nariuchi, A. Matsuzawa, and T. Kakiuchi. 1998. A novel mutant gene involved in T-lymphocyte-specific homing into peripheral lymphoid organs on mouse chromosome 4. *Blood.* 91:2886–2895.

Nitta, T., S. Nitta, Y. Lei, M. Lipp, and Y. Takahama. 2009. CCR7-mediated migration of developing thymocytes to the medulla is essential for negative selection to tissue-restricted antigens. *Proc. Natl. Acad. Sci. USA.* 106:17129–17133. doi:10.1073/pnas.0906956106

Ohnmacht, C., A. Pullner, S.B. King, I. Drexler, S. Meier, T. Brocker, and D. Voehringer. 2009. Constitutive ablation of dendritic cells breaks self-tolerance of CD4 T cells and results in spontaneous fatal autoimmunity. *J. Exp. Med.* 206:549–559. doi:10.1084/jem.20082394

Piccirillo, C.A., and E.M. Shevach. 2004. Naturally-occurring CD4$^+$CD25$^+$ immunoregulatory T cells: central players in the arena of peripheral tolerance. *Semin. Immunol.* 16:81–88. doi:10.1016/j.smim.2003.12.003

Proietto, A.I., S. van Dommelen, P. Zhou, A. Rizzitelli, A. D'Amico, R.J. Steptoe, S.H. Naik, M.H. Lahoud, Y. Liu, P. Zheng, et al. 2008. Dendritic cells in the thymus contribute to T-regulatory cell induction. *Proc. Natl. Acad. Sci. USA.* 105:19869–19874. doi:10.1073/pnas.0810268105

Sakaguchi, S., T. Yamaguchi, T. Nomura, and M. Ono. 2008. Regulatory T cells and immune tolerance. *Cell.* 133:775–787. doi:10.1016/j.cell.2008.05.009

Sha, W.C., C.A. Nelson, R.D. Newberry, D.M. Kranz, J.H. Russell, and D.Y. Loh. 1988. Positive and negative selection of an antigen receptor on T cells in transgenic mice. *Nature.* 336:73–76. doi:10.1038/336073a0

Spence, P.J., and E.A. Green. 2008. Foxp3$^+$ regulatory T cells promiscuously accept thymic signals critical for their development. *Proc. Natl. Acad. Sci. USA.* 105:973–978. doi:10.1073/pnas.0709071105

Sugimoto, N., T. Oida, K. Hirota, K. Nakamura, T. Nomura, T. Uchiyama, and S. Sakaguchi. 2006. Foxp3-dependent and -independent molecules specific

for CD25$^+$CD4$^+$ natural regulatory T cells revealed by DNA microarray analysis. *Int. Immunol.* 18:1197–1209. doi:10.1093/intimm/dxl060

Sugiyama, T., H. Kohara, M. Noda, and T. Nagasawa. 2006. Maintenance of the hematopoietic stem cell pool by CXCL12-CXCR4 chemokine signaling in bone marrow stromal cell niches. *Immunity.* 25:977–988. doi:10.1016/j.immuni.2006.10.016

Tai, X., M. Cowan, L. Feigenbaum, and A. Singer. 2005. CD28 costimulation of developing thymocytes induces Foxp3 expression and regulatory T cell differentiation independently of interleukin 2. *Nat. Immunol.* 6:152–162. doi:10.1038/ni1160

Takahama, Y. 2006. Journey through the thymus: stromal guides for T-cell development and selection. *Nat. Rev. Immunol.* 6:127–135. doi:10.1038/nri1781

Thornton, A.M., P.E. Korty, D.Q. Tran, E.A. Wohlfert, P.E. Murray, Y. Belkaid, and E.M. Shevach. 2010. Expression of Helios, an Ikaros transcription factor family member, differentiates thymic-derived from peripherally induced Foxp3$^+$ T regulatory cells. *J. Immunol.* 184:3433–3441. doi:10.4049/jimmunol.0904028

Vang, K.B., J. Yang, S.A. Mahmud, M.A. Burchill, A.L. Vegoe, and M.A. Farrar. 2008. IL-2, -7, and -15, but not thymic stromal lymphopoietin, redundantly govern CD4$^+$Foxp3$^+$ regulatory T cell development. *J. Immunol.* 181:3285–3290.

Watanabe, N., Y.H. Wang, H.K. Lee, T. Ito, Y.H. Wang, W. Cao, and Y.J. Liu. 2005. Hassall's corpuscles instruct dendritic cells to induce CD4$^+$CD25$^+$ regulatory T cells in human thymus. *Nature.* 436:1181–1185. doi:10.1038/nature03886

Wu, L., and K. Shortman. 2005. Heterogeneity of thymic dendritic cells. *Semin. Immunol.* 17:304–312. doi:10.1016/j.smim.2005.05.001

Yano, M., N. Kuroda, H. Han, M. Meguro-Horike, Y. Nishikawa, H. Kiyonari, K. Maemura, Y. Yanagawa, K. Obata, S. Takahashi, et al. 2008. Aire controls the differentiation program of thymic epithelial cells in the medulla for the establishment of self-tolerance. *J. Exp. Med.* 205:2827–2838. doi:10.1084/jem.20080046

Ziegler, S.F., and Y.J. Liu. 2006. Thymic stromal lymphopoietin in normal and pathogenic T cell development and function. *Nat. Immunol.* 7:709–714. doi:10.1038/ni1360

A Novel DC Therapy with Manipulation of MKK6 Gene on Nickel Allergy in Mice

Megumi Watanabe[1,2], Naozumi Ishimaru[1]*, Meinar Nur Ashrin[1,2], Rieko Arakaki[1], Akiko Yamada[1], Tetsuo Ichikawa[2], Yoshio Hayashi[1]

1 Department of Oral Molecular Pathology, Institute of Health Biosciences, The University of Tokushima Graduate School, Tokushima, Japan, **2** Department of Oral Maxillofacial Prosthodontics, Institute of Health Biosciences, The University of Tokushima Graduate School, Tokushima, Japan

Abstract

Background: Although the activation of dermal dendritic cells (DCs) or Langerhans cells (LCs) via p38 mitogen-activated protein kinase (MAPK) plays a crucial role in the pathogenesis of metal allergy, the *in vivo* molecular mechanisms have not been identified and a possible therapeutic strategy using the control of dermal DCs or LCs has not been established. In this study, we focused on dermal DCs to define the *in vivo* mechanisms of metal allergy pathogenesis in a mouse nickel (Ni) allergy model. The effects of DC therapy on Ni allergic responses were also investigated.

Methods and Finding: The activation of dermal DCs via p38 MAPK triggered a T cell-mediated allergic immune response in this model. In the MAPK signaling cascade in DCs, Ni potently phosphorylated MAP kinase kinase 6 (MKK6) following increased DC activation. Ni-stimulated DCs could prime T cell activation to induce Ni allergy. Interestingly, when MKK6 gene-transfected DCs were transferred into the model mice, a more pronounced allergic reaction was observed. In addition, injection of short interfering (si) RNA targeting the MKK6 gene protected against a hypersensitivity reaction after Ni immunization. The cooperative action between T cell activation and MKK6-mediated DC activation by Ni played an important role in the development of Ni allergy.

Conclusions: DC activation by Ni played an important role in the development of Ni allergy. Manipulating the MKK6 gene in DCs may be a good therapeutic strategy for dermal Ni allergy.

Citation: Watanabe M, Ishimaru N, Ashrin MN, Arakaki R, Yamada A, et al. (2011) A Novel DC Therapy with Manipulation of MKK6 Gene on Nickel Allergy in Mice. PLoS ONE 6(4): e19017. doi:10.1371/journal.pone.0019017

Editor: Jacques Zimmer, Centre de Recherche Public de la Santé (CRP-Santé), Luxembourg

Received January 7, 2011; **Accepted** March 14, 2011; **Published** April 22, 2011

Funding: This study was supported in part by a Grant-in-Aid for Scientific Research (Nos. 17109016, 21390518, and 21791901) from the Ministry of Education, Culture, Sports, Science and Technology of Japan, and research grants from Japan Chemical Industry Association (No. LRi 2005CS02). No additional external funding received for this study. The funders had no role in study design, data collection and analysis, decision to publish, or preparation of the manuscript.

Competing Interests: The authors have declared that no competing interests exist.

* E-mail: ishimaru@dent.tokushima-u.ac.jp

Introduction

Metal allergy is an inflammatory disease categorized as a delayed-type hypersensitivity (DTH) reaction, similar to contact dermatitis and eczema [1,2]. This skin disease is induced by a complex process involving immune responses of numerous cell types, and cooperation among these cells is crucial for symptom development [3,4].

Among various metals, nickel (Ni), when used in costume jewelry or dental alloys, is the most frequent cause of contact allergy [5–7]. Ni-specific T cell responses are crucial for the development of allergies in human and mouse models [8–10]. However, it is unclear how T cells recognize Ni presented to them by antigen-presenting cells (APCs). In the skin, Langerhans cells (LCs) or dermal dendritic cells (DCs) play fundamental roles as APCs for uptake, processing, and presentation of antigens [11,12]. Although there is no evidence that DCs or LCs can directly clear Ni, these APCs may contribute to a Ni allergic response via other molecular mechanisms.

Ni ions (Ni^{2+}) are known to be released from various alloys into the skin and exert proinflammatory and irritant properties as potent allergens or haptens [13,14]. Ni penetrates the skin where it may associate with epithelial cells or become attached to MHC molecules on LCs or DCs. APCs are activated by certain cytokines such as IL-1β and TNF-α produced by keratinocytes. The cytokines regulate the expression of E-cadherin and chemokines like matrix metalloproteinase (MMP)-9, secondary lymphoid tissue chemokine (SLC), and MIP-3β produced by the APCs [15–18]. Subsequently, APCs migrate to draining lymph nodes where they present haptens to naïve T cells. Re-exposure to the same hapten leads to a hypersensitivity reaction in an effector phase.

Recent *in vitro* experiments have reported that contact sensitizers like Ni activate epidermal DCs or LCs as shown by the upregulation of CD80, CD83, CD86, and MHC class II [19]. Moreover, *in vitro* experiments using human DCs showed that Ni-induced phosphorylation of p38 mitogen-activated protein kinase (MAPK) was critical for the maturation of immature DCs [20–22]. In addition, the conditional induction of a dominant active form of MAP kinase kinase 6 (MKK6) efficiently induced the activation of human LCs [23]. However, it remains uncertain whether the *in vivo* activation of DCs in the skin is induced by Ni via the MAPK signaling pathway. Furthermore, it is unclear whether the signaling pathway of DCs stimulated by Ni is different from that of the other stimuli with regard to signal strength or the pathway itself.

The aim of this study was to determine the signaling pathway for APC activation in dermal immune responses related to the pathogenesis of Ni allergy in a mouse model. In addition, a therapeutic strategy based on the *in vivo* molecular mechanisms of Ni allergy was applied to this model.

Results

Induction of Hypersensitive Reactions to $NiCl_2$

To induce hypersensitive reactions to Ni, Ni is typically applied to the skin surface as a secondary challenge after sensitization. In the first series of experiments, we evaluated results of the mouse ear swelling test, as described previously [24]. Using this protocol (Figure 1A), we found flare reactions and slight increases in ear swelling in response to $NiCl_2$ (Figure 1B).

In order to elucidate the symptoms associated with hypersensitive reactions to $NiCl_2$, we administered intradermal injections into the ear pinnae of mice as previously described [25]. Although attempts to induce Ni allergy in mice have often failed, a DTH reaction to Ni has been achieved after injecting $NiCl_2$ in combination with an adjuvant or irritant [25]. Thus, we attempted to induce DTH by injecting $NiCl_2$ in combination with either incomplete Freund's adjuvant (IFA) or complete Freund's adjuvant (CFA) (Figure 1C). A DTH reaction to $NiCl_2$ was induced in C57BL/6 (B6) female mice using the method shown in Figure 1C.

Briefly, $NiCl_2$ with IFA was intraperitoneally injected into B6 mice for initial immunization. Two weeks later, $NiCl_2$ together with CFA was intradermally injected into the ear skin for a recall immune response. DTH reactions were determined by measuring the changes in ear thickness 48 hours after the challenge.

Although increased ear thickness of Ni-treated mice after injection of Ni with IFA has been previously reported [25], in this study, ear swelling was only around 0.2 to 0.3 mm (Figure 1D). In contrast, the ear thickness of Ni+CFA-treated mice after Ni with IFA was significantly higher compared with that of CFA-treated and other mice (Figure 1D). Redness and swelling of the ear skin was observed in Ni+CFA-treated mice after Ni with IFA (Figure 1E). Histological examination of the ear epidermis of Ni+CFA-treated mice after Ni with IFA showed edema, congestion, and extensive infiltration of inflammatory cells, including mononuclear cells, monocytes, neutrophils, and macrophages, in the connective and muscular tissues; however, there was no inflammation in control ears (Figure 1F, Figure S1A). In addition, toluidine blue-positive cells, including degranulated mast cells, found in the lesions of Ni allergy mice were significantly increased compared with those in control mice (Figure S1B). This Ni allergy model with severe inflammation was used to analyze the cellular mechanisms and to develop a therapeutic strategy.

Cellular Mechanisms of Ni Allergy

To characterize Ni allergy, immune responses to another antigen or metal were compared with Ni immune responses in the present allergy model. Briefly, $NiCl_2$ or the control metal/antigen (PBS, ovalbumin [OVA], or TiO_2 [Ti]), along with IFA, was intraperitoneally injected into B6 mice. Titanium has been known as one of biocompatible metals, and so it is believed that the allergic sensitivity induced by nickel is rarely occurred by titanium [26]. Therefore, titanium was used as a control metal in this study. Two weeks later, $NiCl_2$ or the abovementioned control metal/antigen, along with CFA, was intradermally injected into the mice. At 24 and 48 hours after immunization, DTH reactions were assessed by measuring ear thicknesses. In contrast to the swelling seen in OVA- or Ti-treated mice, the ear thicknesses of Ni-treated mice were significantly increased at both 24 and 48 hours after the second challenge (Figure 2A).

Flow cytometry was performed to identify the phenotypes of infiltrating lymphocytes in the allergic lesions. Large numbers of $CD3^+$ T cells and $CD19^+$ B cells were detected in the tissue samples obtained from $NiCl_2$-injected mice (Figure 2B). In addition, immunohistochemical analysis indicated that a much higher proportion of $CD3^+$ T cells were observed in the skin tissues of $NiCl_2$-injected mice, compared with $CD19^+$B cells (Figure 2C). The infiltrating T cells were largely $CD4^+$ T cells, with small numbers of $CD8^+$ T cells and $NK1.1^+$ natural killer (NK) cells (Figure S2A). Moreover, the proportion of NKT cells reactive to anti-α-GalCer-CD1d complex in the ear tissues of $NiCl_2$-injected mice was significantly increased compared with that of control mice (Figure S2B). The number of MHC class II^+CD11c^+ dermal DCs was significantly higher in $NiCl_2$-injected mice than in control mice (Figure 2D). In addition, the absolute numbers of dermal DCs in $NiCl_2$-injected mice were significantly increased compared with those in control mice (Figure 2E). In contrast, the number of DCs in the cervical lymph nodes of Ni-injected mice was not increased (Figure S2C). These results suggest that T cells and dermal DCs in the skin lesions play important roles in the development of the hypersensitivity reaction induced by $NiCl_2$.

Activation of DCs by $NiCl_2$ via MAPK

Numerous signaling molecules control the maintenance of DCs in peripheral tissues [27]. Among these, MAPK is known to be a key signal transducer for the activation of DCs in various immune responses [28,29]. Regarding DCs in allergic reactions in humans, p38/MKK6 in the MAPK pathway plays a significant role in the activation of DCs during the development of skin allergy [23]. Thus, we focused on p38/MKK6 of DCs in mice. To define *in vivo* p38/MKK6 activation of dermal DCs in our Ni allergy model, Western blot analysis of MKK6 was performed using skin tissue samples. MKK6 phosphorylation was significantly increased in the skin tissues of $NiCl_2$-injected mice (Figure 3A), but absent in the skin tissues of PBS-, OVA-, and TiO_2-injected mice (Figure 3A). Further, phospho-MKK6 was detected in MHC class II^+ DCs in the skin tissues of $NiCl_2$-injected mice (Figure 3B). These results showed that dermal DC activation via MKK6 was important for the pathogenesis of Ni allergy in the skin.

On the other hand, when phosphorylation of MKK6 and p38 in bone marrow-derived cells (BMDCs) stimulated with $NiCl_2$ was examined by Western blot analysis, the phosphorylated levels of MKK6 and p38 in $NiCl_2$-stimulated BMDCs were elevated similar to those in LPS-stimulated BMDCs (Figure S3A). When stimulated with TiO_2, however, no phosphorylation of MKK6 and p38 was detected (Figure S3A). We used real-time PCR to examine the MKK6 mRNA expression in BMDCs stimulated with $NiCl_2$. The mRNA expression level of MKK6 in BMDCs stimulated with $NiCl_2$ was increased in a time-dependent manner; it was much higher than that in LPS-stimulated BMDCs during the first 24 hours (Figure S3B), but decreased after 36 hours (Figure S3B). These results showed that Ni could directly trigger the activation of DCs via p38/MKK6 to induce an allergic immune reaction.

Enhanced Allergy after Transfer of T Cells Primed by $NiCl_2$-stimulated DCs

As shown in Figure 2, a large number of T cells had infiltrated into the lesions of inflamed skin tissues. In addition, when purified T cells from the lymph nodes of the Ni allergy model were stimulated with anti-CD3 mAb, production of Th1-type cytokines, including IL-2 and IFN- γ, was significantly increased compared

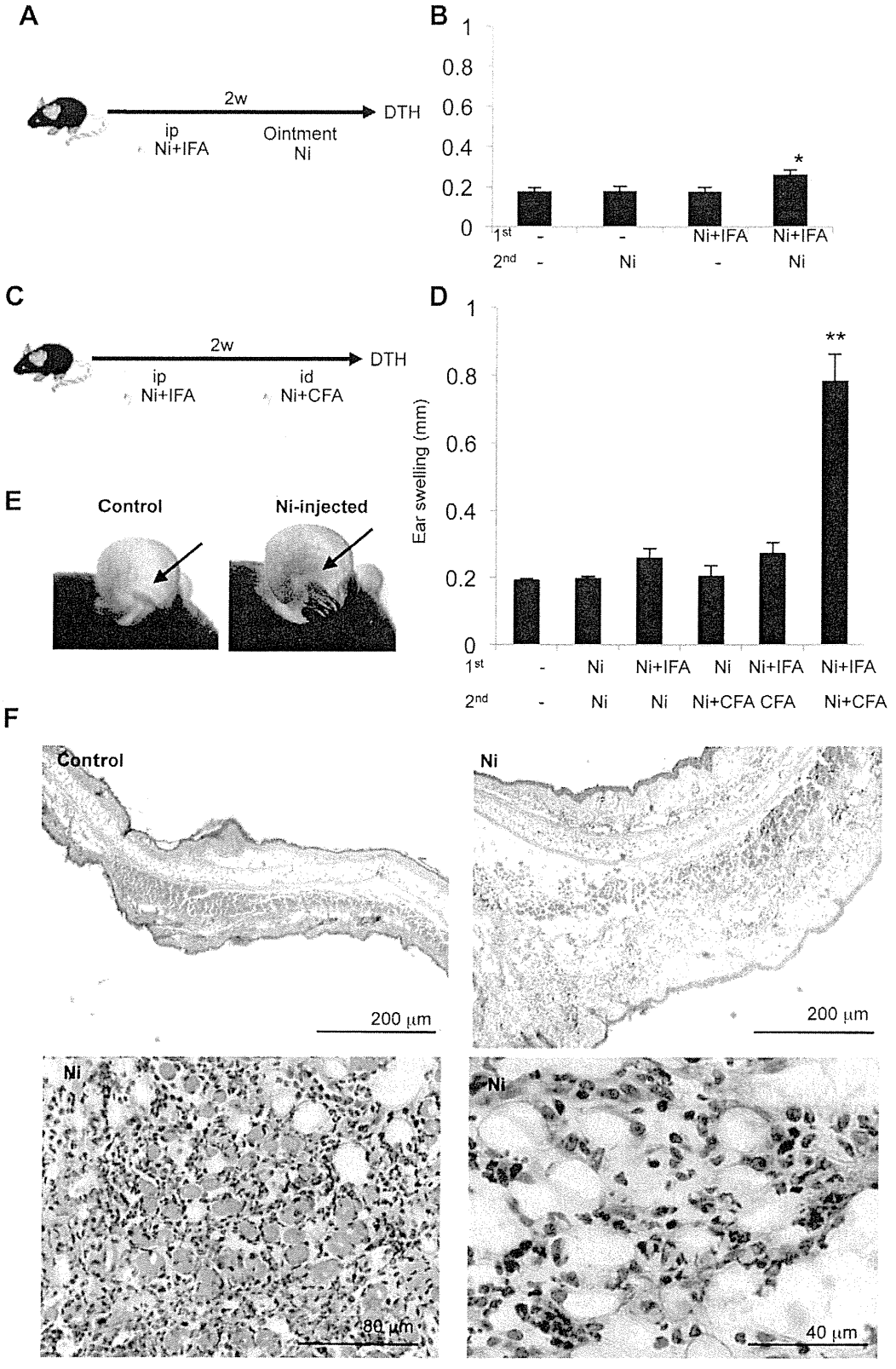

Figure 1. Induction of Ni allergy. (A) Protocol for inducing the Ni allergy model. First, an intraperitoneal injection of $NiCl_2$ with or without IFA was administered. After 2 weeks, an ointment (o) of $NiCl_2$ with Vaseline was applied to the ear pinnae as a secondary challenge. (B) DTH was assessed by measuring the ear thickness at 48 hours after the last challenge. Results are means ± SD for 4 mice in each group. (C) Protocol for inducing a Ni allergy model. First, an intraperitoneal injection of $NiCl_2$ with or without IFA was administered. Then, after 2 weeks, an intradermal injection of $NiCl_2$ with or without CFA was administered to the ear pinnae to induce a secondary reaction. (D) DTH was assessed by measuring the ear thickness at 48 hours after the last challenge. Results are means ± SD for 4 to 6 mice in each group. $^{**}P<0.005$. (E) Representative photos of the ears from control and $NiCl_2$-injected mice. (F) Histological images of inflammatory lesions in the skin are representative of 5 mice in each group.
doi:10.1371/journal.pone.0019017.g001

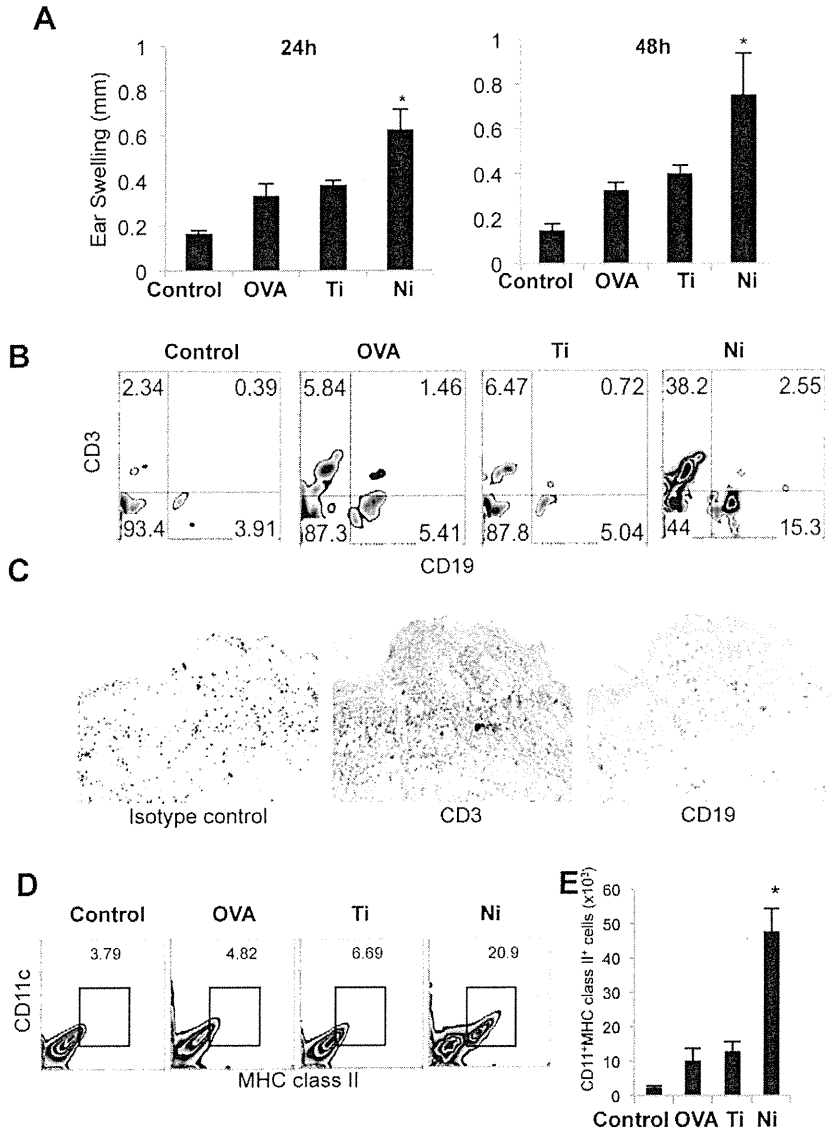

Figure 2. Characteristics of the Ni allergy model. (A) DTH was evaluated by measuring the ear thickness of the treated mice. Results are means ± SD for 5 mice in each group. *$P<0.05$. (B) T and B cell populations of purified lymphocytes from skin tissues were analyzed by flow cytometry. Representative results of 5 mice in each group are shown. (C) Immunohistochemical analysis of T and B cells was performed on frozen sections of inflamed ear tissues obtained from Ni allergy mice. Representative photos of 2 independent experiments are shown. (D) Dermal DCs were detected by flow cytometry. These results represent 2 independent experiments with 3 mice in each group. (E) The absolute numbers of dermal DCs were determined. *$P<0.05$.
doi:10.1371/journal.pone.0019017.g002

with that in controls (Figure S4). On the other hand, the secretion of Th2-type cytokines such as IL-4 and IL-10 from anti-CD3 mAb-stimulated T cells of Ni allergy model was similar to that of the other control mice (Figure S4). These findings suggest that T cells play a key role as effector cells in the pathogenesis of Ni allergy. However, it was still unclear how Ni-stimulated DCs were related to T cell responses in allergic reactions.

Thus, T cells purified from the spleens of normal B6 mice were co-cultured with Ni-stimulated BMDCs *in vitro* for 24 hours. Then, the resulting primed T cells were transferred intraperitoneally into normal B6 mice, and 2 weeks later, $NiCl_2$ with CFA was injected intradermally to induce DTH (Figure 4A). The skin thickness of the model mice with transferred Ni-BMDCs-stimulated T cells was significantly increased compared with that of mice with transferred nonstimulated T cells (Figure 4B). Pathological examination of the skin lesions in the mice with transferred Ni-BMDCs-stimulated T cells showed more severe inflammation, including lymphocyte infiltration, edema, and congestion, compared with those in the mice with transferred nonstimulated T cells (Figure 4C). These results suggested that the T cells primed by Ni-stimulated DCs were important for the onset of Ni allergy.

Effects of Overexpression of MKK6 in DCs on Ni Allergy

To examine whether DCs activated by the engagement of p38/MKK6 signaling influenced the development of skin allergy, BMDCs were transfected with the MKK6 gene (MKK6-DC) and stimulated with $NiCl_2$ for 48 hours. Then, MKK6-DCs were subcutaneously transferred into normal B6 mice, and 2 weeks later, $NiCl_2$ was intradermally injected to induce Ni allergy (Figure 5A). The skin redness in MKK6-DC-transferred mice was

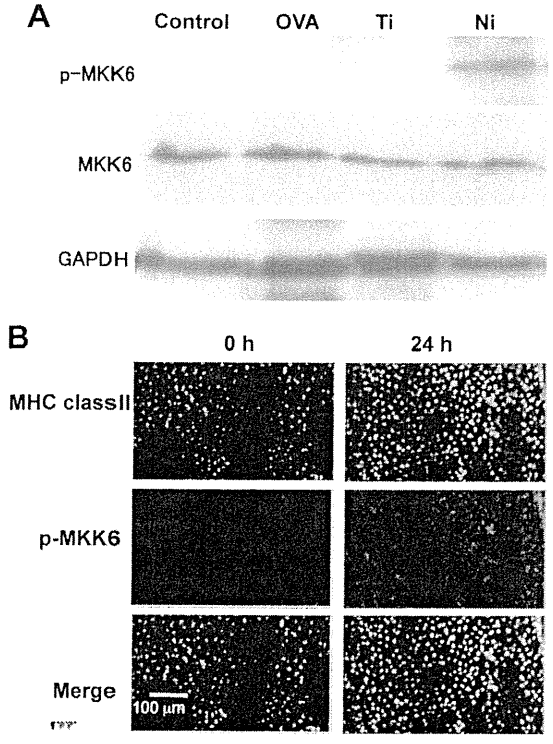

Figure 3. DC activation by Ni via MKK6. (A) Phosphorylation of MKK6 in the inflamed tissues of the Ni allergy model was analyzed by Western blot analysis. GAPDH was used as the internal control. (B) Phosphorylation of MKK6 (Red) of MHC class II^+ (Green) dermal DCs from Ni allergy mice was detected by confocal microscopy. These results represent 2 independent experiments with 3 to 5 mice in each group.
doi:10.1371/journal.pone.0019017.g003

enhanced compared with that in Mock-DC-transferred mice (Figure 5B). In addition, pathological examination revealed remarkable infiltration of immune cells along with congestion and edema in the skin lesions of MKK6-DC-transferred mice (Figure 5C). Significantly enhanced ear swelling was detected within 48 hours of injecting $NiCl_2$ into MKK6-DC-transferred mice compared with Mock-DC-transferred mice (Figure 5D). In addition, we investigated production of cytokines by Ni-stimulated DCs that are required for T cell priming, including IL-12, IFN-γ, and IL-10. The amounts of IL-12, IFN-γ, and IL-10 produced by BMDCs after stimulation with $NiCl_2$ were equal to those after stimulation with LPS (Figure S5), and the cytokine production by $NiCl_2$-stimulated BMDCs were significantly higher compared with that by TiO_2-stimulated BMDCs (Figure S5). These results suggested that Ni-mediated DC activation played a central role in T cell priming for the onset and development of Ni allergy.

Effective Therapy for Ni Allergy using MKK6 siRNA

We next tested a therapeutic strategy for Ni allergy using short interfering (si) RNA targeting the MKK6 gene. Before inducing a DTH reaction, MKK6 siRNA with atelocollagen as an *in vivo* gene delivery system was subcutaneously injected into the ear skin of the model mice. Ear thickness was measured at 48 hours after injecting $NiCl_2$ or saline control (Figure 6A). We confirmed that the MKK6 mRNA level in siRNA-treated DCs was significantly reduced (<1/6) compared with that in control siRNA-treated DCs (data not shown).

Ear thickness of MKK6 siRNA-treated allergy model mice was significantly reduced compared with those of control siRNA-treated mice (Figure 6B). In addition, pathological examination showed no detectable inflammatory lesions in MKK6 siRNA-treated mice, while severe inflammation with extensive lymphocytic infiltration, edema, and congestion was observed in the lesions of the mice injected with control siRNA (Figure 6C). Further, although phosphorylation of MKK6 of MHC class II^+ dermal DCs in the skin sheets from MKK6 siRNA-treated mice was nearly undetectable, there was phosphorylation in the sheets from control siRNA-treated mice (Figure 6D). This showed that an effective therapy using siRNA targeting the MKK6 gene could be used for treating Ni allergy.

Discussion

DCs in the epidermis and dermis participate in the recognition of pathogens. The two major populations of DCs present in normal skin are epidermal LCs and dermal DCs. These DCs function as APCs and play key roles in sensing pathogens and initiating allergic responses. Immature DCs, such as epidermal LCs, reside in the peripheral tissues. When these DCs are activated by antigens and mature, they migrate from peripheral sites to lymphoid organs where they stimulate T cells to induce an immune response [11,30]. The cutaneous immune system depends on multiple cell-cell contacts for antigen recognition and presentation, as well as inflammation. LCs facilitate the development of contact hypersensitivity responses by efficiently presenting haptens to T cells [31]. However, it has been suggested that dermal DCs can support LC functions [31].

From our results and those of other studies, allergy symptoms, such as swelling and flare reactions, were minimal and transient after applying a Ni-based ointment to the skin surface. Artik et al. demonstrated contact hypersensitivity in model mice after intradermally injecting Ni into the ear pinnae [25]. Our method using intradermal injections of Ni with CFA in a new DTH model was based on their report. Clinical skin tests (such as puncture tests and intradermal injection tests) along with patch tests have been used for the diagnosis of metal allergy. Therefore, we injected $NiCl_2$ with CFA intradermally into mice in order to obtain clear hypersensitivity responses.

p38 MAPK is an evolutionarily highly conserved stress response pathway in various cells [32]. p38 MAPK is activated by an upstream kinase (MKK6 or MKK3) and then translocated into the nucleus where target molecules are phosphorylated by p38 MAPK [33,34]. A previous report showed that activation of human LCs was triggered by MKK6 [23]. In addition, several reports using *in vitro* experiments showed that p38 MAPK phosphorylation played an important role in the activation of DCs by Ni [34–36]. Our experiments using a Ni allergy model strongly suggest that MKK6 phosphorylation in dermal DCs is the first important trigger for the onset of an allergic response to Ni.

Ni is the most frequent cause of metal allergy. It is possible that Ni in the skin may interact with proteins, after which dermal DCs capture the Ni–antigen complex. At this stage, Ni might be a potent factor for triggering activation of DCs via MKK6. In our model, the specific activation of MKK6 in DCs was observed only when the cells were stimulated with Ni but not another metal or antigen such as Ti or OVA. However, because the phosphorylation of MKK6 in DCs was detectable after stimulation with LPS *in vitro*, the signaling pathway induced by Ni could be modulated by other stimuli. In addition, we could not identify the mechanism by which Ni modulated MKK6 expression.

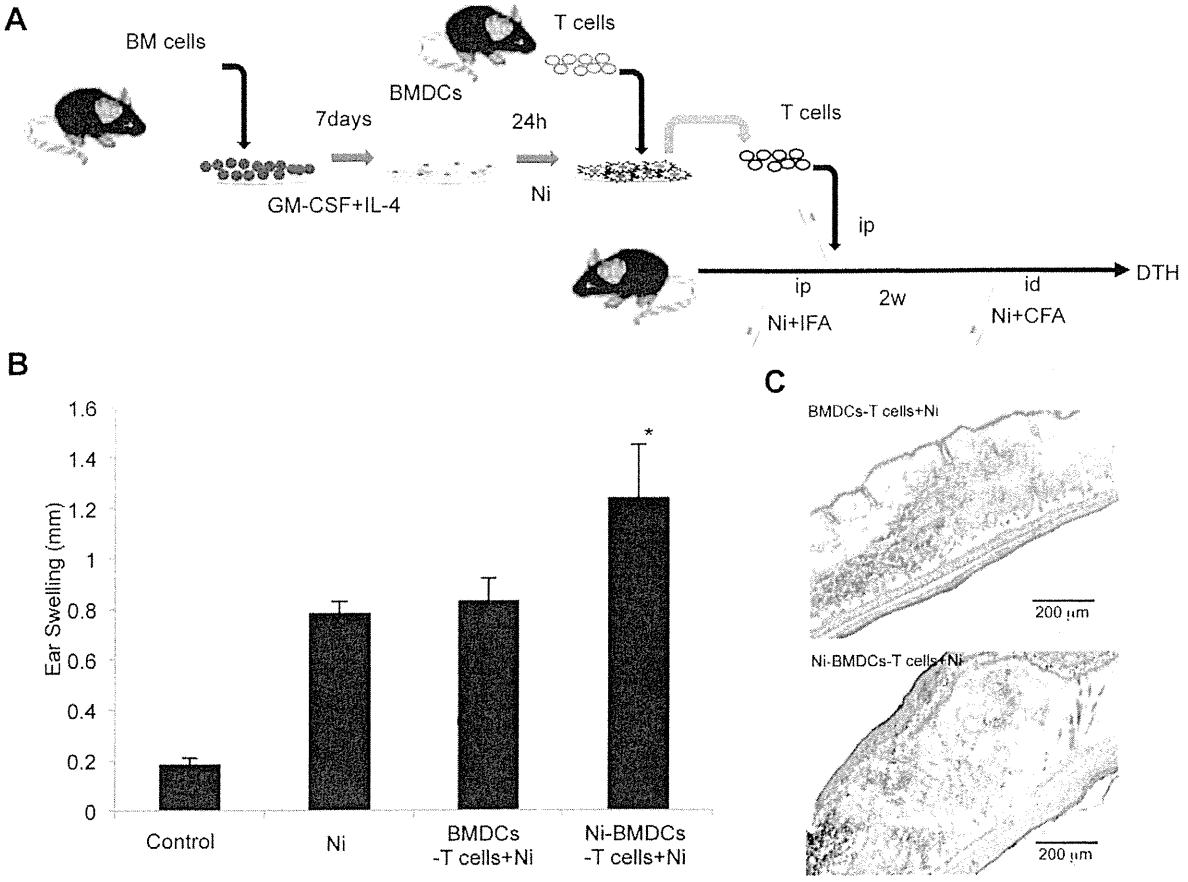

Figure 4. Effect of T cell transfer on DTH in the Ni allergy model. (A) Purified T cells from the spleens of B6 mice were co-cultured with BMDCs in the absence (control) or presence of $NiCl_2$ for 48 hours and then intraperitoneally transferred into B6 mice. DTH reaction was induced by injecting $NiCl_2$. (B) Ear thickness was measured at 48 hours after the challenge. Results are means ± SD for 5 mice in each group. *$P<0.05$. (C) Inflammatory lesions of the mice with transferred Ni-DC-stimulated T cells.
doi:10.1371/journal.pone.0019017.g004

It was recently reported that human Toll-like receptor (TLR) 4 plays a crucial role in the development of contact allergy to Ni [37] and that only TLR4-deficient mice expressing transgenic human TLR4 developed contact hypersensitivity to Ni, while animals expressing mouse TLR4 did not develop DTH. Although the cell type contributing to a TLR4-mediated allergic reaction was not identified, immune cells such as DCs, macrophages, and endothelial cells were associated with an allergic reaction to Ni via TLR4. It is possible that TLRs other than TLR4 are related to Ni allergy in mice. In our mouse model, although the signaling pathway via TLR in DCs was not examined, MKK6 phosphorylation was observed in LPS-stimulated DCs *in vitro*. Thus, cooperative or synergistic actions of Ni with other signaling pathways, including TLR, following MKK6 activation may be associated with Ni allergy in this mouse model. Our *in vivo* experiments suggested that DCs activated by Ni enhanced T cell migration to local lesions and T cell-dependent allergic response; however, it remains unclear how Ni can stimulate or control DC activation via MKK6. Moreover, our result showed that significantly increased number of NKT cells reactive to anti-ααGalCer-CD1d complex was found in the ear lesion of Ni model mice. CD1d-restricted NKT cells have been referred to as natural memory cells in both innate and acquired immune responses [38]. However, the relationship between metal allergy and the role of NTK cell has been still unidentified. Further research using our model will be necessary for understanding the cellular mechanism of metal allergy.

DC maturation can be initiated by inflammatory stimuli, such as cytokines, LPS, CD40 ligation, and contact allergens [39]. Activated DCs take up antigens and produce a variety of cytokines and chemokines, which in turn attract and activate eosinophils, macrophages, and NK cells to the site of antigen entry [30]. After antigen capture, DCs migrate to regional lymph nodes and present peptide-MHC complexes to antigen-specific T cells that induce T cell-dependent immune responses, such as Ni allergy [40]. Interestingly, our results showed a significantly increased number of dermal DCs in the skin tissues of mice with Ni allergy. These findings suggest that circulating precursor DCs might accumulate at the $NiCl_2$ injection site. Moreover, the experiments using skin tissues demonstrated that phosphorylation of MKK6 in dermal DCs and LCs was clearly detectable. These results indicated that stimulation with Ni enhanced both accumulation and activation of DCs.

DCs are activated by signaling via pattern recognition receptors (PRRs), such as TLRs and retinoic acid-inducible gene I-like receptors, in response to a variety of ligands [41,42]. PRR signaling leads to the activation of nuclear factor (NF)-κB. Although it is unclear whether Ni can interact with receptors such as PRRs, previous reports showed that the differentiation of human DCs is promoted by Ni via NF-κB activation [43,44]. It

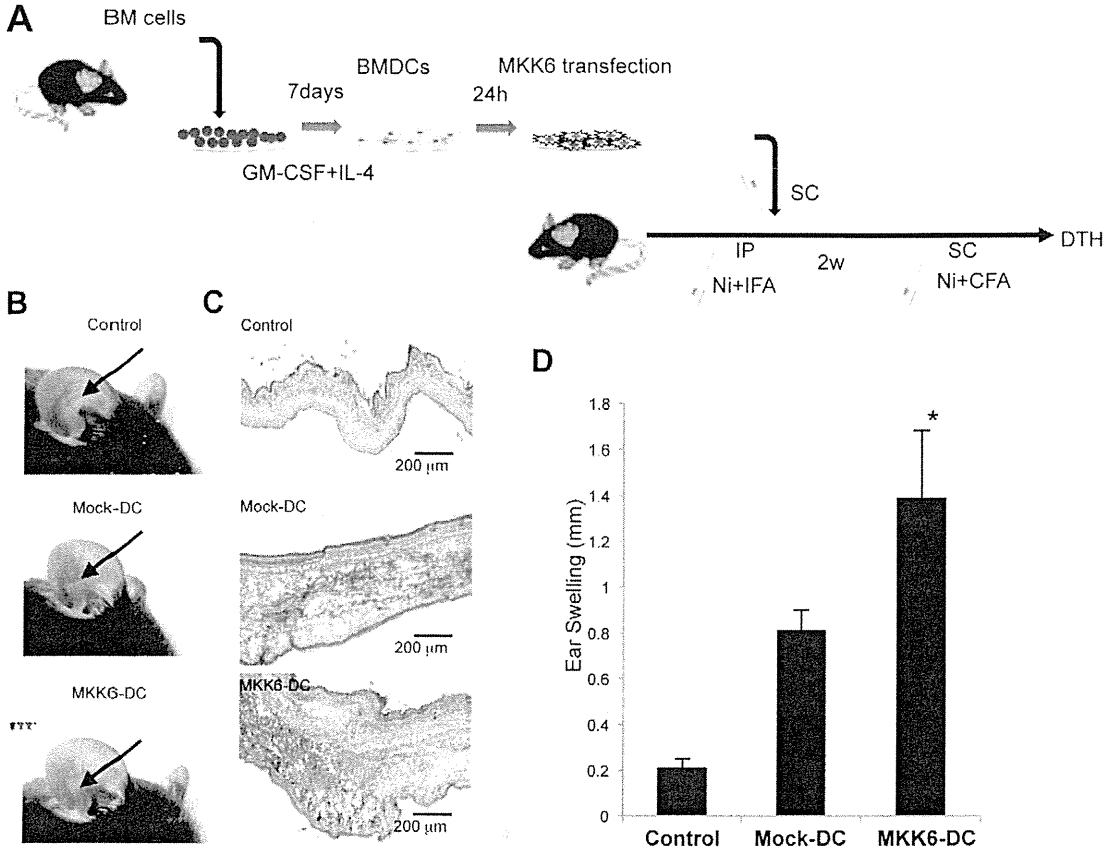

Figure 5. Effect of DC transfer on the Ni allergy reaction. (A) MKK6 DNA or mock plasmids were transfected into BMDCs. MKK6/DCs or Mock/DCs were subcutaneously injected into B6 mice. The mice were challenged with $NiCl_2$ to induce DTH. (B) Representative photos are shown for 3 to 5 mice in each group. (C) Inflammatory lesions of the mice with transferred MKK6/DCs. These results are representative of 2 independent experiments with 3 mice in each group. (D) Ear thickness was measured at 48 hours after the challenge. Results are means ± SD for 5 mice in each group. *$P<0.05$.
doi:10.1371/journal.pone.0019017.g005

remains uncertain whether NF-κB signaling plays a role in the pathogenesis of metal allergy.

Our *in vivo* experiments demonstrated that manipulating the MKK6 gene of DCs could control Ni allergy. Many reports on DC therapy for cancer or infection have indicated that antigen presentation to T cells by DCs is important for controlling these diseases [14,45,46]. However, there are no reports regarding DC therapy for metal allergy. Our new approach with siRNA targeting the MKK6 gene could be a powerful strategy for the prevention and cure of metal allergy. Careful attention should be paid to the therapeutic effects of MKK6 inhibition on the immune system in the treatment of allergic immune responses.

In conclusion, the signaling pathway via p38/MKK6 plays a key role in activating dermal DCs in the pathogenesis of metal allergy. DC therapy using MKK6 gene manipulation could be effective for treating metal allergy. Characterization of this cellular mechanism could have clinical implications by supporting the development of new diagnoses or treatments for these allergic diseases.

Materials and Methods

Ethics

This study was conducted according to the principles expressed in the Declaration of Helsinki. The study was approved by the Institutional Review Board of the University of Tokushima (toku09021).

Mice

Female C57BL/6J mice (6–8 weeks old) were purchased from CLEA Japan, Inc (Tokyo, Japan). All mice were maintained in specific pathogen-free conditions in our animal facility.

Histology and Immunohistochemistry

Skin was removed from the mice, fixed with 10% phosphate-buffered formaldehyde (pH 7.2), and prepared for histological examination. Formalin-fixed tissue sections were stained with hematoxylin and eosin. Immunohistochemistry was performed for freshly frozen sections by the biotin-avidin immunoperoxidase method using an avidin-biotin immunoperoxidase complex reagent (Vector Laboratories, Burlingame, CA, USA). Monoclonal antibodies against CD3 and CD19 (eBioscience, San Diego, CA, USA) were used.

Induction of Ni Allergy

Ni allergy was induced using a modification of a method described previously [24,25]. To induce a hypersensitivity reaction to Ni, 25 μl of 1 μmol/ml $NiCl_2$ with 25 μl of IFA (ICN Biomedicals, Inc., Aurora, OH, USA) was intraperitoneally injected into B6 mice for initial immunization. Two weeks later, mice were administered intradermal injections of Ni,

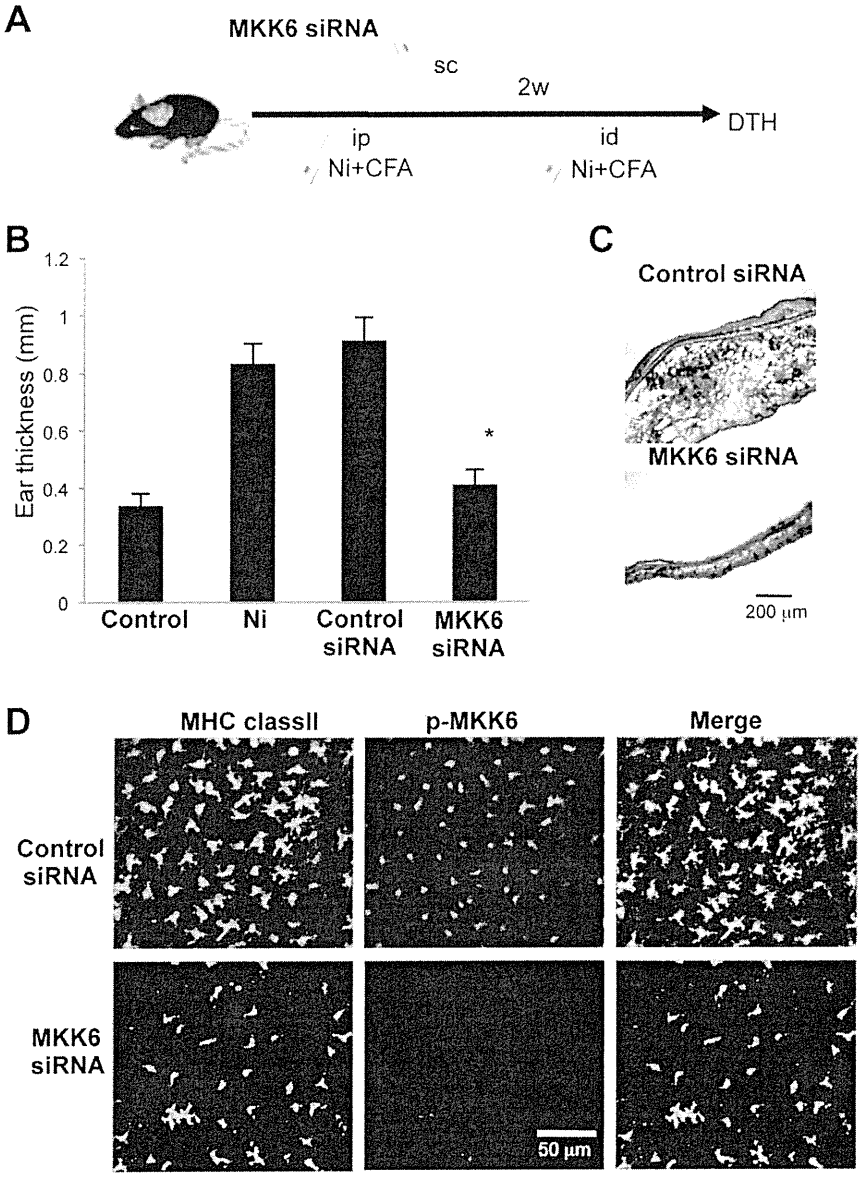

Figure 6. DC therapy for Ni allergy. (A) siRNA for MKK6 with atelocollagen was subcutaneously injected into the ear skin of Ni allergy mice. (B) Ear thickness was measured at 48 hours after injecting $NiCl_2$. Results are means ± SD for 5 mice in each group. *$P<0.05$. (C) Pathological findings after *in vivo* administration of MKK6 siRNA and control siRNA. (D) Phosphorylation of MKK6 of MHC class II^+ dermal DCs was analyzed by confocal microscopy. These results are representative of experiments with 5 mice in each group.
doi:10.1371/journal.pone.0019017.g006

10 μl of 0.2 μmol/ml $NiCl_2$ with CFA (ICN Biomedicals, Inc.) using 28G1/2 needles (TERUMO Tokyo, Japan) for a recall immune response. DTH reactions were determined by measuring the changes in ear thickness at 24 or 48 hours after the challenge [25].

DC Preparation

DCs were prepared from freshly isolated bone marrow cells as described previously [26]. Briefly, bone marrow cells were seeded in 6-well culture plates (Nunc A/S, Roskilde, Denmark) in RPMI-1640 medium supplemented with 10% heat-inactivated FCS, 2 mM L-glutamine, 100 U/ml penicillin, and 100 μg/ml streptomycin, and then incubated for 1 hour at 37°C in a humidified 5% CO_2 atmosphere. After nonadherent cells were removed, adherent cells were incubated and changed to 1 ml of fresh medium containing 10 ng/ml GM-CSF (R&D System, Inc., Minneapolis, MN, USA) and 1 ng/ml IL-4 (eBioscience) on days 2, 4, and 6. Dermal DCs were prepared from the skin of female B6 mice. Excised skin was cut into small pieces and the dermal side was exposed to 1.0% trypsin at 37°C for 60 minutes. Epidermis was incubated in 0.025% DNase for 20 minutes at room temperature. After an equal volume of RPMI was added, the solution was swirled for 5 minutes and filtered using a 70 μm cell strainer (BD Biosciences, Franklin Lakes, NJ, USA). The dermal cell suspension that included DCs was washed three times with RPMI, and the resulting pellet was re-suspended. Dermal DCs were enriched by centrifugation using Opti-prep (Invitrogen, Carlsbad, CA, USA).

Flow Cytometry

Expression levels of surface markers were examined by staining 1×10^6 cells with 1 μg/ml of antibodies against CD3, CD4, CD8, CD19, CD11c, and MHC class II conjugated with either FITC or PE (eBioscience). Cells were analyzed on FACScan (BD Biosciences).

Western Blot Analysis

Samples of stimulated or nonstimulated DCs were subjected to sodium dodecyl sulfate-polyacrylamide gel electrophoresis (SDS-PAGE) with 10% acrylamide gel, transferred onto a polyvinylidene fluoride (PVDF) membrane (Bio-Rad Laboratories, Hercules, CA, USA), and the blotted membranes were incubated with anti-MKK6, phospho-MKK6 (Cell Signaling Technology, Inc., Denver, MA, USA), or glyceraldehyde-3-phosphate dehydrogenase (GAPDH) (Santa Cruz Biotechnology, Inc., Santa Cruz, CA, USA) mAbs. Immune complexes were detected using horseradish peroxidase (HRP)-conjugated anti-mouse IgG (Bio-Rad Laboratories) and ECL-plus reagents (Amersham Bioscience Corp. Piscataway, NJ, USA).

MKK6 Plasmid Construction and Transfection

MKK6 cDNA obtained from RT-PCR was subcloned into an expression vector, pcDNA3.1 (Invitrogen). Transient transfections were carried out using a jet-PEI Mannose reagent (Poly transfection, Illkirch, France) before stimulation. DCs were transfected with the MKK6 plasmid, and then stimulated with either 1 μmol/ml $NiCl_2$ or 1 μmol/ml TiO_2 for 48 hours.

siRNA for MKK6

MKK6 and control scramble siRNA reagents were obtained from B-bridge International, Inc. (Sunnyvale, CA, USA). Sequences of the oligonucleotides were as follows: MKK6: sense, 5′-CUACAGUAGUGAAGAGAUUTT-3′; antisense, 5′-AAUCUCUUCACUACUGUAGTT-3′ and control: 5′-ATCCGCGCGATAGTACGTA-3′. Using the *in vivo* siRNA transfection kit AteloGene (KOKEN, Tokyo, Japan), siRNA was injected into ear skin according to the manufacturer's instructions [47]. In brief, 10 μM siRNA was mixed with AteloGene and rotated gently at 4°C for 20 minutes. This solution (20 μl) was subcutaneously injected into the ear pinnae. Five days after injection, ear swelling was evaluated.

Confocal Microscopic Analysis

Skin sheets were isolated from ears of treated mice with 3.8% ammonium thiocyanate, and stained with anti-phospho-MKK6 (Santa Cruz Biotechnology) mAb and MHC class II mAb (eBioscience). These sheets were analyzed using Confocal Laser Microscan (LSM 5 PASCAL; Carl Zeiss. Inc., Oberkochen, Germany).

Statistical Analysis

Results are given as means ± standard deviations (SD). Comparison was done using Student's *t* test or Mann-Whitney *U* test. Differences were considered statistically significant for *P* values of <0.05.

Supporting Information

Figure S1 Inflammatory lesions in Ni allergy model. (A) Edema and inflammatory cell infiltrations were observed in the skin tissues of Ni allergy mice. Photos are representative of five mice in each group. Original magnification is ×100 (upper) and ×200 (lower). (B) The number of toluidine blue$^+$ cells including mast cell in the lesion of Ni allergy model was significantly increased compared to that of control mice. Toluidine blue staining was performed as described in Methods S1. Photos are representative of three mice in each group. Data are means ± SD of 3 mice. *$P<0.05$, vs control.
(TIF)

Figure S2 Flow cytometric analysis of immune cells in Ni allergy model. (A) CD4$^+$ and CD8$^+$ T cells or NK1.1$^+$ cells of ear tissues form controls and Ni allergy models were detected by flow cytometry. Results are representative of three mice in each group. (B) NKT cells of spleen, cervical lymph nodes, and ear tissues were detected by using PE-conjugated anti-αGalCer mAb-CD1d complex. Results are representative of three mice in each group. (C) CD11c$^+$ MHC class II$^+$ DCs in cervical lymph nodes (LNs) from control, OVA, TiO_2, and $NiCl_2$-injected mice were analyzed by flow cytometry as described in Method S1. The results were representative of three to five mice in each group.
(TIF)

Figure S3 Activation of MAPK signaling of DCs by Ni. (A) BMDCs were stimulated with $NiCl_2$, LPS or TiO_2 for 24 hours, phosphorylation of MKK6 and p38, and total MKK6 and p38 protein were detected by Western blot analysis. GAPDH was used as the respective internal control. Results are representative of 3 independent experiments. (B) MKK6 mRNA expression of BMDCs stimulated with $NiCl_2$ or LPS was analyzed by real-time PCR as described in Method S1. Data are shown as relative expressions to β-actin, and are representative of 3 independent experiments.
(TIF)

Figure S4 Cytokine secretions from Ni-stimulated T cells. T cells from cLNs of control, OVA, TiO_2, and $NiCl_2$-injected mice were enriched by negative selection using mAbs (anti-MHC class II, B220, NK1.1, and CD11b) and magnetic beads. The T cells were stimulated with plate-coated anti-CD3 mAb for 24 hours. The secretions of IL-2, IFN-γ, IL-4, and IL-10 in the supernatants were analyzed by ELISA as described in Method S1. Data are means ± SD of triplicates. *$P<0.05$, vs control.
(TIF)

Figure S5 Cytokine secretions from Ni-stimulated DCs. BMDCs were stimulated with $NiCl_2$, LPS, and TiO_2 for 24 hours. The cytokine secretions of IL-12, IFN-γ, and IL-10 were detected by ELISA as described in Method S1. Data are means ± SD of triplicates.
(TIF)

Methods S1
(DOCX)

Acknowledgments

We thank S. Katada, A. Nagaoka, and N. Kino for their technical assistance.

Author Contributions

Conceived and designed the experiments: MW NI TI YH. Performed the experiments: MW NI MNA RA AY. Analyzed the data: MW NI MNA. Wrote the paper: MW NI YH.